Towards better fatigue predictions in large offshore wind turbines: A review of climate, aero-hydrodynamic, and computational approaches

Journal of Ocean Engineering and Science xxx (xxxx) xxx

Contents lists available at ScienceDirect

Journal of Ocean Engineering and Science

journal homepage: www.elsevier.com/locate/joes

Review article

Towards better fatigue predictions in large offshore wind turbines: A review of climate, aero-hydrodynamic, and computational approaches

Gabriele Mangia [a,*], Michele Martini [b], Giuseppe Giorgi [a], Giovanni Bracco [a]

[a] Marine Offshore Renewable Energy Lab (MOREnergy Lab), Department of Mechanical and Aerospace Engineering (DIMEAS), Politecnico di Torino, Corso Duca degli Abruzzi 24, Torino, 10129, Italy

[b] ENI S.P.A, Via Felice Maritano 26, San Donato Milanese, 20097, Italy

ARTICLE INFO

Keywords:
Offshore wind
Fatigue
Damage
Renewable energy

ABSTRACT

The rapid increase of offshore wind turbines size has made fatigue calculation a critical design and assessment challenge. Increasing turbine dimensions, hub heights, and environmental exposure introduce significant uncertainty across all the steps of fatigue assessment, while detailed long-term simulations remain computationally demanding.

This review aims at providing a structured overview of the engineering-standard framework used for fatigue prediction in large offshore wind turbines, encompassing climatological characterization, load evaluation, and fatigue damage calculation. Across the entire estimation chain – from wind and wave data characterization and modeling, through aerodynamic and hydrodynamic load evaluation, to structural modeling and fatigue assessment – multiple commonly adopted approaches are systematically reviewed and compared.

In addition, the review explicitly discusses, for all the above-mentioned sections, the trade-offs between modeling fidelity and computational cost associated with different methodological choices, highlighting their impact on fatigue predictions.

By adopting this broad, system-level perspective aligned with engineering practice and design standards – rather than focusing exclusively on latest academic development – this work supports informed method selection for design optimization, iterative assessment procedures, and fatigue-oriented design of large offshore wind turbines.

1. Introduction

The current climatological and geopolitical context is forcing countries and governmental unions to act in order to reduce the carbon dioxide emissions. This represents an ultimate attempt to contain the global warming well below +2 °C with respect to the pre-industrial age (Paris Agreement) [1].

Energy production is one of the main drivers of increasing CO_2 emissions, accounting for almost 75% of the total [2]. Despite the recent progress, achieving a CO_2-free energy system remains challenging, as meeting net-zero targets implies a substantial large-scale deployment of renewable generation rather than marginal increases. According to the International Energy Agency (IEA) projections, for reaching net-zero emissions by 2050, nearly 70% of global electricity generation should be supplied by solar photovoltaic (PV) and wind energy [3]. Both technologies already play a significant role in renewable electricity production, contributing approximately 18% (solar) and 26% (wind), respectively [4]. However, it is evident that a massive effort is still required.

Concerning wind energy, the path towards the future consists in a rapidly increasing trend for offshore installations. The growth that offshore technologies are witnessing is related to a series of benefits associated to open sea environment.

The first one is a better wind resource, namely usually higher speed and less turbulence with respect to the onshore case, which drastically reduce the fatigue issues of the turbines and allows lower hub heights. The second one is related to the space availability and the reduced impacts on the population in terms of noise and, in some cases, of visual. Being far from urbanized areas can help dealing with people acceptance and can also allow to install bigger units [6]. According to the bathymetry, it is possible to choose between bottom fixed or floating technologies. The first typology is suitable for water depth below 50 m, otherwise the latter is preferred [7].

As previously mentioned, the possibility to install bigger units has fostered companies, universities and research centers to develop concepts of floating wind turbines with rated power of 22 MW and beyond

* Corresponding author.
E-mail address: gabriele.mangia@polito.it (G. Mangia).

https://doi.org/10.1016/j.joes.2026.02.009
Received 2 December 2025; Received in revised form 5 February 2026; Accepted 25 February 2026
Available online 2 March 2026

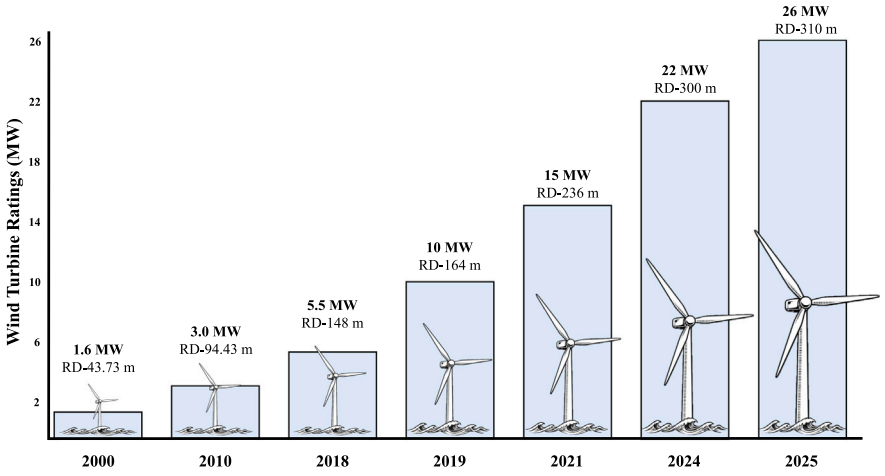

Fig. 1. Offshore wind turbine size growth.
Source: adapted from [5].

(e.g. IEA [8]). Meanwhile, in China, 18 MW turbines have already been installed and now a 26 MW has been tested [9–11]. This progressive growth of the rated power (Fig. 1) implies longer blades, as well as higher towers, hence higher forces acting on the structure which can lead to more fatigue damage [12]. Accordingly, it has already been demonstrated that the design phase of large monopiles is lead by the fatigue behavior [13]. Indeed, despite being subject to both wind and wave loading, bottom-fixed turbines' fatigue behavior is dominated by wind loads, especially for large structures [14]. When it comes to floating concepts, in addition to the influence of upscaling dimensions and wind loading, a dominant role is played by the continuous dynamic excitation derived by wave loading and wind-wave coupling phenomena [15–17].

The above-mentioned issues are leading to an ever-increasing attention to the fatigue problem. The reason behind the importance of this calculation relies on costs and downtime losses associated to non-programmed intervention due to fatigue failure [18] and the possibility to avoid them.

The main sources of uncertainties that affect fatigue life estimation are related to climate data, load modeling, material resistance and fatigue assessment approach [19]. Most of the existing review studies address uncertainty-related features by focusing on separate individual stages of the fatigue assessment. A comprehensive overview encompassing all the modeling steps of fatigue prediction is still missing. In particular, current reviews lack a system-level perspective considering how modeling choices performed in each step of the assessment influence the final result of fatigue evaluation. This approach is fundamental for making informed decisions regarding the modeling of the entire fatigue assessment process.

Concerning climatological and environmental modeling, in Toft et Al. (2016) [20] the uncertainties in wind climate estimation and the following impact on the wind turbine loads are addressed. However, the variability evaluation introduced by fatigue evaluation methodologies is missing. In Warder et Al. (2025) [21], the influence of climate change and wake on wind resource is discussed. The focus is posed on the future changes in the distribution of the wind resource, which will influence production and fatigue damage of the turbines. Nevertheless, no real investigation on the structural side is present. In Ramezani et Al. (2023) [22], the discussion is deeply focused on the uncertainties in environmental load evaluation and materials, as well as on uncertainty evaluation methods. On the other hand, the influence of the structural model adopted to mimic the behavior of the structure is not analyzed. Also fatigue evaluation methods are not addressed in this work.

Conversely, other review studies aim at discussing more the mechanical and fatigue assessment side. In Liao et Al. (2022) [23], recent developments and future prospects in the field of wind turbines fatigue are proposed, analyzing in detail the main issues related to the components, without focusing on the environmental loads modeling. In Dong et Al. (2022) [24], the uncertainties in fatigue loads and life for ships and offshore structures is treated in detail, focusing on fatigue modeling. However, minimal reference is shown on the wind and wave or climate change impact in the fatigue estimation, relevant for offshore wind turbines.

As a result of the above discussion, a systematic and integrated assessment of how modeling choices and uncertainties influence the entire fatigue estimation framework is still missing. To address this gap, the present review provides a comprehensive and critical overview of engineering-standard fatigue assessment methodologies. The goal is to examine the combined influence of climatological, aero-hydrodynamic, structural, and fatigue modeling strategies on the accuracy and reliability of fatigue predictions. The focus is posed on the primary structural elements of offshore wind turbines (tower, blades and support structure). For the sake of clarity, the term *'uncertainty'* is defined herein as encompassing the variability in the results of a calculation or in the estimation of a quantity arising from the range of possible approaches and methodologies employed to perform the task.

The remainder of this paper is organized as follow: climatological data uncertainties (Section 2) load evaluation uncertainties (Section 3), fatigue evaluation methods (Section 4), discussion (Section 5) and conclusions (Section 6). A more detailed subdivision of the sources of uncertainties can be found in Fig. 2.

2. Climatological data uncertainties

Generally, wind and wave spectra and time series are used as starting point to evaluate the fatigue loads that the turbine and its support structure must withstand during the entire lifetime. Hence, when evaluating the fatigue damage it is important to be aware also of the uncertainties produced by the differences between the dataset and reality. This point is remarked in [20], where it is shown that the uncertainties related to site specific climate conditions are usually between 10%–30% of the total uncertainty in the structural reliability analyses.

2.1. Wind data

Wind can be defined as the horizontal movement of air from areas of high pressure to areas of low pressure, primarily due to the uneven

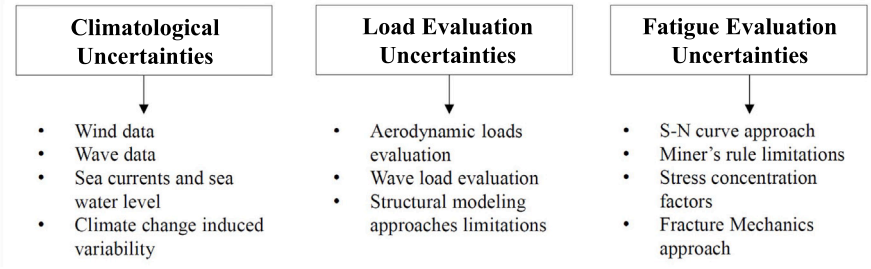

Fig. 2. Uncertainties sources analyzed in this paper.

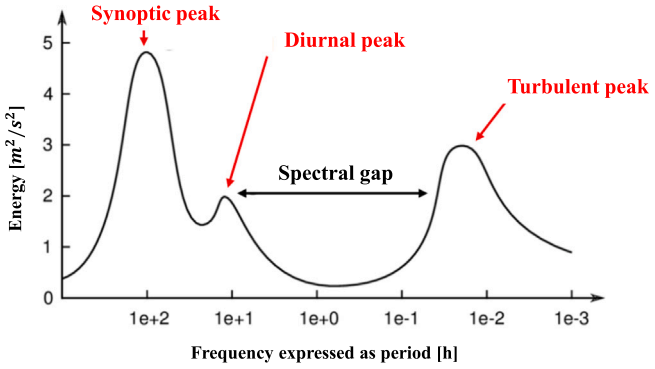

Fig. 3. Wind speed fluctuation spectrum.
Source: adapted from [27].

heating of the Earth's surface by the Sun. It is influenced by several factors as Earth's rotation (Coriolis effect), friction with the surface, and geographic features, which together play a crucial role in determining its speed and direction.

Its variations can be described with the aid of Van Der Hoven spectrum [25], which is characterized by three peaks as shown in Fig. 3. The synoptic peak is the result of synoptic meteorological conditions which usually change in a range of 10 days - 24 h. The diurnal peak is representative of daylight wind increment, hence is located in a range between 24–10 h. The turbulent peak is caused by high-frequency fluctuations which produce those wind variations in the order of tenth of seconds or minutes [26].

The impacts on loads estimation caused by the adopted wind modeling strategy have been investigated in [28]. In this study it is highlighted that the turbulence spectral region has the most significant impact on the loads and consequently on the fatigue life of the wind turbine, as increasing turbulence is associated to higher damage and vice versa [29]. In the context of short-term wind loads modeling, the reference is represented by the use of IEC-61400-1 [30] and DNVGL-ST-0437 [31] standards which suggest the simulation of constant mean flows associated with a turbulence intensity, intended as the variation between the instantaneous value of the wind with respect to its 10-minute average. For fatigue applications, it is recommended to divide the wind speed range in bins of maximum 2 m/s width and to perform ten minutes simulations (each one having its own generation seed) for a minimum total amount of 1 h. The standards suggest two turbulence models that can be used for the design load calculations: Mann uniform shear turbulence model [32] and Kaimal spectrum and exponential coherence model [33]. In the first one, the coherence naturally emerges from the three-dimensional field, while in the second model it is empirically imposed. For this reason, the first one is more physically consistent, but requires a more complex expression and higher computational costs [34]. Both of them are involved in the Normal Turbulence Model (NTM) framework, which prescribes the turbulence standard deviation. In DNV standard [31] this parameter is further discussed taking into account also offshore conditions which are different with respect to onshore ones.

The IEC standard also allows the possibility to use other turbulence models, provided that the related fatigue loads are higher than those obtained using the recommended models. Despite the large agreement for high frequencies, significant differences rise in the lower frequency section of the turbulence spectra. DNV-RP-C205 standard [35] recommends the empirical Ochi and Shin spectrum, the Simiu and Leigh or the Frøya spectrum for offshore ambient. These three spectra have more energy content at lower frequencies but below 0.001 Hz the first one is not calibrated using any measured data, while the third one is based on neutral conditions on the Norwegian sea. It is important to highlight that these models are focused on the description of wind on a short to very-short timescale, hence the very low frequency ($< 10^{-5}$ Hz) synoptic and diurnal peak are omitted [36]. Further details and equations of the most common short-term wind spectra and turbulence models can be found in Appendix.

Very low frequency wind changes are generally taken into account using medium/long term wind probability distributions, Rayleigh or Weibull [37,38]. These statistical representations relies on long-term wind data sources, which play a crucial role in defining the occurrence of slow wind speed variations. Long-term wind characterization is usually based on a combination of in situ measurements, commonly performed using wind masts and lidar systems, together with reanalysis datasets and satellite-based observations. These methodologies provide extended temporal coverage but differ in terms of spatial resolution and local representativeness. While offshore wind masts and lidar measurements offer high accuracy at specific locations [39], their limited temporal extent often restricts their ability to capture multi-year synoptic and seasonal variability. Conversely, reanalysis and satellite datasets enable long-term characterization of wind climate but may fail in representing local features and extreme events [40,41]. This aspect is particularly critical for large offshore wind turbines, since fatigue appears to be a dominant failure mode for severe weather events like typhoons [42,43].

In standard fatigue assessment engineering frameworks, short-term time-domain simulation are usually combined with long-term wind speed occurrence in order to estimate fatigue damage. This approach can generate an underestimation of load cycles as seen in [44] where a methodology is developed to take into account even very low frequency fatigue dynamics caused by the slow variations of wind speed (i.e synoptic and diurnal peak driven) which have periods well above the commonly used 10 min signals. In [45,46], a validation of a corrective factor to account for very low frequency dynamics is presented. This parameter, called 'ratio of damage' converges to a constant increasing the days of observation. In [47] the influence of atmospheric conditions on the spectrum, and consequently on the loads, is investigated using the Højstrup 1981 Unstable Spectra Model [48] finding that in highly unstable environment larger loads are expected, up to 47% more than in neutral conditions.

In the above paragraphs it has been shown that standard short-term wind modeling typically relies on the assumption of Gaussian

statistics. However, wind measurements have demonstrated that real wind time series often deviate from Gaussian behavior, exhibiting intermittency or encompassing skewed probability distributions. To address this limitation, recent research has explored Non-Gaussian wind modeling approaches (e.g., [49]). These methodologies have predicted higher loading, especially for extreme weather conditions, which has translated into higher blade crack propagation rates.

In parallel, data-driven technologies based on Machine Learning (ML) have been intensively investigated both for wind data modeling and long term resource characterization. Rather than replacing physical models, these approaches are primarily used for reanalysis downscaling, fusion of multiple wind data sources, and reconstruction of wind statistics for partially sampled locations. Additional information concerning the applications of Artificial Intelligence (AI) – in particular ML – on wind data, can be found in [50,51].

2.2. Wave data

In contrast to onshore installations, offshore wind turbines are subjected to additional hydrodynamic forces, necessitating the integration of wave modeling for a comprehensive and accurate load assessment. A common mathematical description of the phenomenon begins with the definition through the Airy linear theory [52] of the expression for a single, regular sinusoidal wave which can be represented by the equation:

$$\eta(t) = a\sin(\omega t + \phi) \tag{1}$$

where η represents the free surface elevation, ϕ the wave phase, $a, T \subset R^+$ are respectively the wave amplitude and period with $a = H/2$ and H the height of the wave. $\omega = 2\pi/T$ is the wave angular frequency. The apparent confusion of the sea can be represented, as a first approximation, using a superposition of a large number (N) of regular sinusoidal waves [53].

$$\eta(t) = \sum_{i=1}^{N} a_i \sin(\omega_i t + \phi_i) \tag{2}$$

Moreover, it is reasonable to assume that for time periods between 20 min to 6 h (e.g., in the short term) the sea surface is stationary [35]. Given these features, for a short term time series of the free surface elevation it is possible to obtain a spectral density function. Some of the most widely used are the Pierson-Moskowitz spectrum [54], mostly suitable for fully developed seas, and the JONSWAP spectrum [55] which is used for growing seas. They can be represented by (3) and (4) as per [56]:

$$S_\omega(\omega) = \frac{\alpha g^2}{\omega^5} exp[-\beta\frac{\bar{\omega}_\omega^4}{\omega^4}] \tag{3}$$

$$S_\omega(\omega) = \frac{\alpha g^2}{\omega^5} exp[-\beta\frac{\bar{\omega}_\omega^4}{\omega^4}]\gamma^{a(\omega)} \tag{4}$$

where $\alpha, \beta \subset R^+$ are constant values, g is the acceleration of gravity, $\bar{\omega} = 2\pi/\bar{T}_\omega \in R^+$ is the peak-frequency, and $a : R^+ \rightarrow R^+$ is the exponent of the peak-shape parameter, depending on the frequency ω.

Accordingly, it is possible to characterize the short term sea state using only a set of parameters as the significant wave height H_s, defined as the average height of the highest one-third waves in the analyzed period, and the peak period T_p, which can be calculated as the inverse of the frequency at which the peak of the spectrum is registered. The JONSWAP spectrum contains also a peak shape parameter γ: its value can be tuned from 1 to 7. For $\gamma = 1$ the JONSWAP spectrum reduces to the Pierson-Moskowitz. The tuning of the parameter γ represents itself a source of uncertainty: in [35] an average value of $\gamma = 3.3$ is proposed, even though it is highly recommended the use of site-related data to find a more reliable value of γ [57]. An example of JONSWAP spectra for varying γ is shown in Fig. 4. Indeed, other spectra have been proposed in literature, including two peaks spectra for locations where

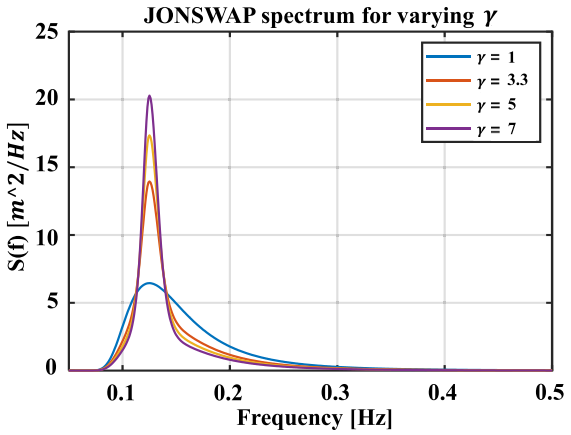

Fig. 4. Jonswap Spectrum for varying γ.

two dominant wave systems with different peak frequency are present (usually wind and swell waves) [58,59].

Another important issue associated to wave data and modeling is the multi-directionality. Waves are usually described through unidirectional spectra, leading to uncertainties both in power production evaluation of wave energy converters [60], as well as in the offshore structures loading. Actually, in irregular sea states, the wave components come from several directions; therefore, to account for this phenomenon, the wave spectrum can be modified to become function of two parameters, the frequency ω and the direction θ [61], as per Eq. (5)

$$S(\omega, \theta) = S(\omega)D(\theta, \omega) \tag{5}$$

where $S(\omega)$ is the frequency dependent spectrum, while $D(\theta, \omega)$ is the directional spectrum whose integral is equal to 1. For additional information about this spectrum, [60,62,63] are recommended. In [64], considering multidirectionality can lead to fatigue damage reduction of 40/60% with respect to the unidirectional approximation.

After the analysis of the short term, it is necessary to extend the analysis to the long term. To do so, in wave analysis is common the adoption of scatter plots: these graphs are matrices characterized by a discretization for the two main wave parameters, H_s and T_p, and for each couple of values an occurrence is associated. To obtain this data it is possible to use several methods: satellite data, in-situ buoy measurements or reanalysis models (e.g., ECMWF Reanalysis v5 known as ERA5) sometimes coupled with a third generation wave model like SWAN (Simulating WAves Nearshore) [65]. In particular, third generation wave models are spectral models that emulate the evolution of the sea-state without imposing a predefined spectral shape, but solving the wave action balance equation. These models are able to consider wind energy input, non-linear wave interactions and additional phenomena which allow for a more physically consistent representation of wave conditions.

Indeed, there are several uncertainties related to these approaches. Reanalysis models bring temporal and spatial resolution issues (e.g., ERA5 provides hourly data, spatially distributed in a 31 km grid [66]) hence they cannot accurately characterize waves in a small area [67] and they do also require proper calibration [68]. However, they are able to provide global coverage as well as great reliability. Despite world-wide coverage, satellite data are subject to revisit time, namely the time required by the satellite to pass again over a certain location. This can lead to the loss of short term meaningful events and their misrepresentation. They can be also disturbed by objections on sea surface, by salinity, sea ice and resolution decreases if the target area is expanded [69]. In-situ buoy measurements may suffer of reliability issues of the instruments as they can be damaged by vessel

Table 1
Qualitative comparison of accuracy, reliability, cost-effectiveness, spatial/temporal resolution, and coverage for wave data collection methods.

Method	Accuracy	Reliability	Cost-Effectiveness	Spatial/Temporal Resolution	Coverage
Satellite data	++	++	+++	++/+	+++
Reanalysis models	+/++	+++	+++	+/++	+++
In-situ measurements	+++	++	+	+++/+++	+

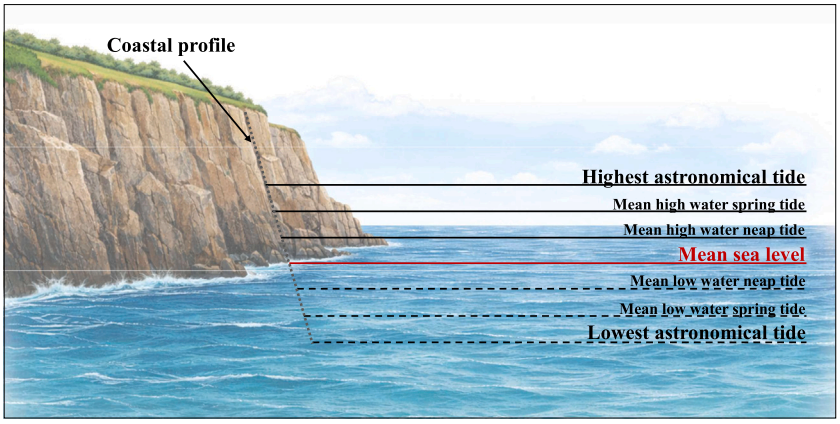

Fig. 5. Tides ranges.

or debris and extreme meteocean conditions, mooring system requires maintenance. On the other hand, they can provide local data with high temporal resolution and high accuracy but at higher costs. A qualitative comparison of the methodologies is resumed in Table 1.

Recent advances in wave modeling show a progressive integration of data-driven and hybrid approaches combining ML techniques to physics-based models. This methods can be used to reconstruct missing data [70], improve predictive capabilities [71] as well as increase the fidelity of spectral representation [72]. Despite being very promising, these techniques still lack of a regulatory framework and standardization. For this reason, these approaches may be used for complementary analyses.

2.3. Sea currents and sea water level

Sea currents can be mainly divided into tidal currents and wind driven currents, despite additional components (e.g., storm surges) may be present. Tidal currents are associated to astronomical forces and appear concurrently with the rise and fall of water sea level [22]. Wind-driven sea currents, at the surface level, can be estimated as a fraction of wind speed $U_{wind} = kV_{wind}$ with values of k from 0.016 to 0.033. For increasing water depths [31] suggests to approximate the wind driven current using a linear decreasing behavior. Sea water level is subjected to tidal, wind and pressure fluctuations. Usually, the astronomical tidal range is described as the variation between the highest astronomical tide and the lowest astronomical tide (Fig. 5), while its average is defined as mean sea level.

It is also possible to observe intermediate water levels caused by the variations in the gravitational forces acting on water masses. In particular, spring tides occur when the Sun, Moon, and Earth are aligned (during full moon and new moon), causing a greater tidal range than usual. Neap tides are the opposite of spring tides. They are observed when the Sun and the Moon form a 90° angle relative to the Earth (during the first and last quarter phases of the Moon). In this configuration, the gravitational pull of the Sun partially cancels out that of the Moon, reducing the tidal range. The highest sea water level can be reached when a positive storm surge is coupled to the highest astronomical tide, vice versa the lowest sea water level is reached when a negative storm surge is coupled with the lowest astronomical tide.

Concerning the effects that current and tides have on fatigue calculations, in [73] an increase on fatigue load is observed for the case in which current and waves are opposite, while a reduction is expected when they are aligned. In addition to this, in [15] it is highlighted the importance of wave–current interaction that can lead up to 15% variation in substructure fairlead tensions, which may enhance fatigue damage. For the changes in sea water level, standards like DNVGL-ST-0437 [31] do not prescribed particular study on this aspects, recommending normal water sea level ranges.

2.4. Climate-change effects on data

The evidence that the world is undergoing deep changes from a climatological perspective has already been presented in the introduction chapter. Since the majority of the studies related to offshore wind turbines is currently performed using datasets that describe the climatological environment from a certain point in the past up to the present, a discussion is open in literature on the reliability of this data to predict future climatological means and extremes. Most of the studies that have been conducted are based on the Shared Socioeconomic Pathways (SSP) SSP 2–4.5, SSP3-7.0 and SSP5-8.5, which represent human development based on socio-economic features that still increase greenhouse gas emissions at least in the medium term (Fig. 6).

In [74] for 2–4.5 (SSP2-4.5), a reduction of 5%–15% wind potential across Europe is forecast, while for SSP5-8.5 the reduction reaches even 10%–20%. Also in [75,76] an overall reduction of the European wind potential is expected, in particular for the Mediterranean basin. In [77] the north America region is investigated, with results showing a decrease up to 15%–20%, in line with previous investigations performed by [78]. Nevertheless, there are also regions in which an increase of the wind power density is forecast: in [77,79] higher values up to +10% are expected for Canadian west coast and Hudson bay. Hence, it is evident that in the productivity assessment, but also in the structural design including the fatigue behavior, it is crucial to account for the forecast changes in wind speed and potential. In [80], the climate change effect on wind and on fatigue calculation has been investigated using a surrogate model. Results show that fatigue damage on a monopile structure is more impacted than the energy production when climate change effect is introduced. However, these simulations are subject to several uncertainties, such as biased initial conditions, imperfect model physics, downscaling issues [81] which can alter the final results. For this reason, it is difficult to provide a standardized framework to take into account the phenomenon rather than using safety factors.

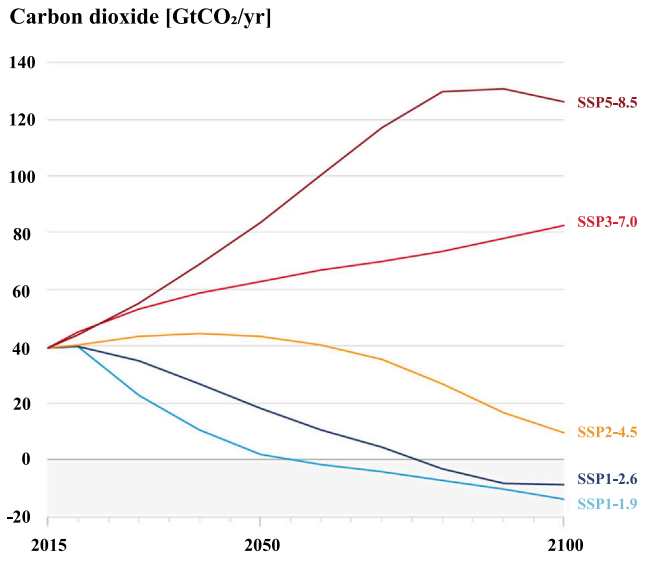

Fig. 6. Carbon dioxide emission trends and relative SSP [82,83].

3. Load evaluation uncertainties

Offshore wind turbine loads are generated by the combined action of aerodynamic, hydrodynamic, and structural effects and represent a key driver for design and lifetime assessment. As already mentioned in the introduction chapter, according to the bathymetry the support structure can be bottom-fixed or floating. These two technological options exhibit fundamentally different dynamic responses. Bottom-fixed turbines are primarily governed by aerodynamic excitation and wave-induced loads [14]. In addition to this, floating wind turbines experience platform motions that strongly couple aerodynamic and hydrodynamic loads [17]. Consequently, the latter require aero-hydro-servo-elastic simulations to capture complex coupling effects.

Hence, load evaluation and the associated uncertainties depend both on the environmental conditions but also on the adopted turbine and foundation concept, as well as on the modeling assumptions used to represent the underlying physical processes. For this reason, in the following sections a review of the standard modeling frameworks employed to describe aerodynamic loading, wave-induced loads, and structural response, is presented. Moreover, emerging techniques aimed at improving load prediction, uncertainty quantification and reducing computational costs, are reported.

3.1. Aerodynamic loads evaluation

Aerodynamic loads on offshore wind turbines are generated by the interaction between the atmospheric flow and the rotating blades. They are influenced by a variety of factors, including wind field characteristics and control strategies. In particular, turbine control systems – as pitch and torque control – play a central role in regulating aerodynamic loading. By continuously adjusting the rotor response to changing wind conditions, they affect load amplitudes influencing fatigue damage. Additional information on this topic can be found in [84,85].

However, an accurate modeling of the interaction between wind–turbine remains essential for reliable load predictions and can be addressed using different aerodynamic modeling frameworks. Four methods are generally employed: Blade Element Momentum theory (BEM), Boundary Element method (BE), Free Vortex Wake method (FVWM) and Computational Fluid Dynamics (CFD) [86].

BEM theory is at the base of wind turbine aerodynamics modeling given its low computational cost and the good reliability of the results,

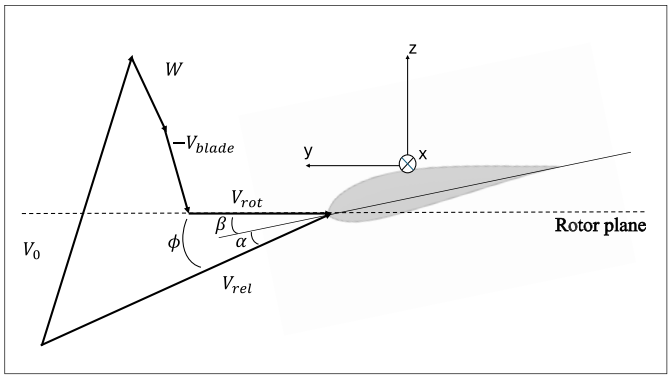

Fig. 7. Construction of velocity vectors.

providing that sufficiently good airfoil data are used for lift and drag coefficients as function of the attack angle and Reynolds number [87]. The methodology is based on the possibility to independently consider 10–20 sections along the rotor, where a wind speed loss is established between the front and the rear of the foil. This reduction is derived by the extraction of power through the axial forces, generated by the pressure gradient over the blade section. However, BEM approach is based on some simplifying assumptions: the static pressure drop driven by wake rotation is not considered, as well as the radial velocity. This leads to some inconsistencies between this theory and reality, hence additional corrections can be applied to increase the accuracy as in [88].

In Fig. 7 it is possible to see the velocity triangle representing the vectors involved in the BEM theory. V_o is the undisturbed wind speed, V_{rot} is the rotor speed, W is the induced velocity, namely the additional wind field generated by the action of the loads [87]. V_{blade} is the blade velocity without the component generated by rotor rotation (the minus sign accounts for the reference systems, set on the blade section) while V_{rel} is the wind relative velocity with respect to the blade. The figure shows also the angle of attack α and the flow angle ϕ. It is therefore possible to extract the induced velocity components and then the thrust coefficient C_T [87]:

$$W_z = \frac{-BLcos\phi}{4\rho\pi rF|V_0 + f_g \cdot \mathbf{n}(\mathbf{n}\cdot\mathbf{W})|} \tag{6}$$

$$W_y = \frac{BLsin\phi}{4\rho\pi rF|V_0 + f_g \cdot \mathbf{n}(\mathbf{n}\cdot\mathbf{W})|} \tag{7}$$

$$C_T = \frac{dT}{1/2\rho V_0^2 dA} = 4aF(1 - f_g \cdot a) \tag{8}$$

where B is the number of blades, L is the lift force, $a = \frac{W_z}{V_0}$ is the axial interference factor, and f_g is the Glauert correction for turbulent wake state and F is Prandtl's tip loss correction. To further increase the accuracy of BEM based codes, which usually overestimate the blade loading by 15%–20% [89], empirical corrections to model root losses, nonuniform inflow, unsteady inflow, and skewed flow have been introduced as well as adjustments to extend the validity also in turbulent wake state and vortex ring state [90]. Nevertheless, the complexity is increased when it comes to floating wind turbines, because of the additional vibrations generated by the platform and by the presence of the turbine in its own wake [91].

These physical challenges can be handled by using CFD methodologies, commonly used to obtain complex aerodynamic results like wake flow features and complex inflow conditions [86]. CFD can accurately solve and obtain the required information of the flow by solving Navier–Stokes equation, at the expense of computational cost. Nonetheless, some aspects still need to be improved: for example, the turbulence model requires corrections using empirical parameters and the method is dependent on the experience of mesh generation [91].

Table 2
Qualitative comparison of standard aerodynamic load modeling approaches for offshore wind turbines. (*if corrections are implemented).

Method	Core assumptions	Physical behaviors captured	Computational speed	Accuracy
BEM	Inviscid, steady flow; annular independence	Axial induction; empirical wake rotation*	+++ (real-time capable)	+/++*
FVWM	Inviscid, irrotational flow; free wake	Wake convection, rotation; radial velocity	++ (minutes–hours)	++
CFD	Viscous Navier–Stokes, fully resolved	Separation, turbulence, complex wake dynamics	+ (hours–days)	+++
BE	Inviscid, potential flow; blade singularities	Unsteady loads; wake-induced velocities	++ (minutes–hours)	++

Another methodology that is used to deal with floating wind turbine aerodynamics is the family of FVWMs. This methods are based on a Lagrangian approach, meaning that the turbine wake is discretized in Lagrangian markers; this representation can be performed using several methods (e.g., lattice method, filament method etc.). For a complete understanding of the methodology, more material can be found in [92]. Under unsteady flow conditions, FVWMs perform better compared to BEM methodologies [93] but remaining less computationally expensive than CFD [94] and its reliability has been widely confirmed. Moreover, despite generally overestimating aerodynamic loads, in large yaw misalignment conditions, BEM tends to underestimate the blade loads up to 30% with respect to the FVWM [94].

Finally, the BE method is based on the potential flow theory and it is valid provided that the flow is irrotational, inviscid and incompressible. This methodology is rarely used for aerodynamic simulation of wind turbines [95] while widely employed for hydrodynamics and it is treated more in detail in the next paragraph. A more concise comparison can be found in Table 2.

3.2. Wave load evaluation

The evaluation of the loads on the structure caused by incoming waves and their dynamics is defined as hydrodynamic modeling and can be performed using several methodologies, each of them suitable for a certain typology of event and introducing more or less complexities. In particular, it is possible to adopt either a linear approach, generally suitable for small/moderate wave conditions or a non-linear one, which is more common for the analysis of extreme events [96]. Clearly, solving a non-linear model requires more computational effort with respect to the linear one. On the other hand, it is able to produce more accurate results. In the next paragraphs, an overview of the most common strategies is presented which are then resumed in Table 3.

3.2.1. Linear methodologies

The most common linear approach to evaluate the wave–structure interaction is the *linear potential flow theory*. Herein, starting from Bernoulli and Continuity equations and under the hypothesis of incompressible fluid, frictionless (inviscid) and irrotational flow, it is possible to describe the velocity through the definition of a potential function ϕ, so that $v = \nabla\phi$ (as resumed in Fig. 8). To solve the equations for ϕ it is necessary the coupling with appropriate boundary conditions:

- *Linear dynamic boundary condition*:
  fluid pressure must be equal to atmospheric pressure at the undisturbed free surface boundary;
- *Linear kinematic boundary condition*:
  surface velocity and the normal component of fluid particles velocity at the undisturbed free surface boundary must be equal;
- *Impermeability of the body*:
  the fluid particle velocity at the boundary of the body must be the same as the normal component of body velocity;
- *Flatness and impermeability of the seabed*:
  at the seabed, the normal component of fluid velocity must be equal to zero;
- *Wave field decaying far from the body*.

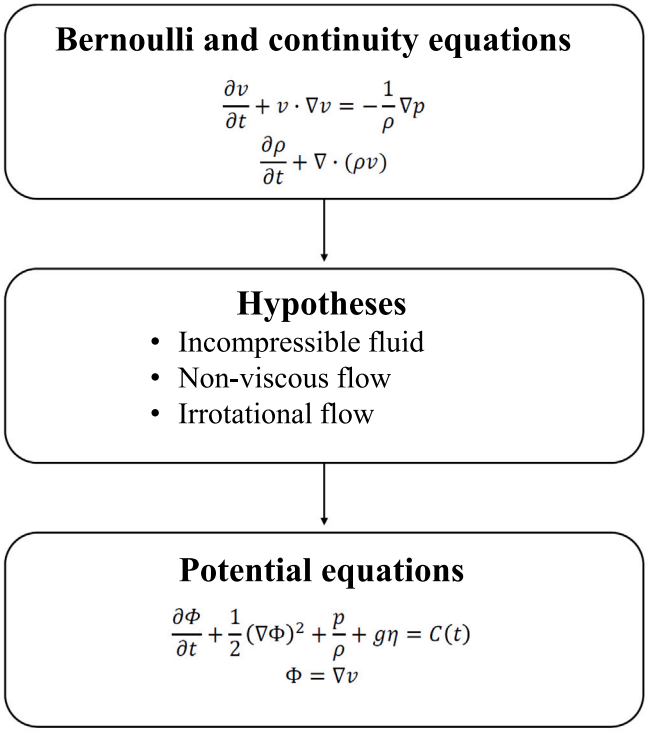

Fig. 8. Flow chart for linear potential flow theory.

If the reader is interested in exploring further details about the meaning of the previous equations, more insights can be found in [56]. The potential flow equation coupled with the boundary conditions is solved to extract the hydrodynamic characteristics in case of floating substructures. To do so, solvers based on Boundary Element methods are widely used in literature, such as ANSYS AQWA [97], WAMIT [98], NEMOH [99]. All the solvers based on these methods are characterized by the integration of the potential equation over the wet surface of the body and a small portion of free water area, discretized through a mesh. The main sources of error/uncertainty for these solvers are *numerical errors*: they are divided into *round-off, iteration and discretization errors*. The latter are the direct consequence of the approximation of partial differential equation into discrete and algebraic ones. Since discretization depends on the mesh size, refining the mesh is useful to reduce this type of errors [100]. As the wave can be divided into three components, *incident, radiated, diffracted*, also the forces and the moments exerted on the body and obtained through the integration of the potential, can be categorized into two classes: *excitation* (Froude–Krylov and diffraction) *forces* and *radiation forces*. To complete the dynamic analysis of the body, the *hydrostatic force* must be considered.

$$\frac{d(m\dot{z})}{dt} = f_e + f_r + f_d \tag{9}$$

where m is the body mass, $\dot{z}$ is the velocity for one of the degree of freedom, f_e, f_r, f_d are the excitation, radiation and diffraction forces.

3.2.2. Non-linear methodologies

When the hypotheses of small/moderate wave conditions are not satisfied, or even for wide oscillation of the body, linear models rapidly

Table 3
Qualitative comparison of standard hydrodynamic load modeling approaches for offshore wind turbines.

Method	Core assumptions	Physical behaviors captured	Computational speed	Accuracy
Linear potential flow	Inviscid, incompressible, irrotational flow; linear free surface	Radiation and diffraction forces; wave excitation; hydrostatic restoring	++ (minutes–hours)	++
Morison equation	Slender body assumption; empirical drag and inertia terms;	Inertial and viscous drag forces;	+++ (real-time capable)	+
Partially non-linear potential flow	Potential flow with selected non-linear free-surface and body-motion terms	Non-linear wave kinematics; weak body–wave coupling	++ (minutes–hours)	++/+++
Fully non-linear potential flow	Inviscid, irrotational flow; fully non-linear free surface boundary conditions	Wave steepening; non-linear wave–structure interaction; higher-order loads	+ (hours)	+++
CFD	Viscous, turbulent flow; fully resolved fluid domain	Wave breaking; slamming; green water; flow separation; viscous effects	+ (hours–days)	+++

become inaccurate [101] and the non-linear hydrodynamics effects must be considered to increase the accuracy of the model. An example of the causes of non-linear behavior are overtopping, slamming, flow separation and viscosity, which derive from the fluid-body interaction [102]. To account for these non-linear effects, it is possible to either use fully non-linear approaches, characterized by high accuracy and computational time, or partially non-linear models, which address only the most influential nonlinearities ensuring less computational burden but lower accuracy [103].

Partial non-linear models are usually based on potential flow methods which include nonlinearities by extending the linear model or considering the Cummins equation as an external load [104]. Fully non-linear methodologies, instead, analyze the interaction fluid-body through the solution of Navier–Stokes equation, which must be performed through a numerical discretization of space and time as it is not possible, up to now, to solve them analytically. The choice depends entirely on the aim of the modeling, as there could be applications in which the computational speed is essential and does not allow long simulations. It is also possible to perform an hybrid approach, coupling CFD and potential flow theory to integrate viscous effects [105,106] and to calculate hydrodynamic coefficients reducing the computational burden [104]. For slender structural geometries, non-linear hydrodynamic loading can be efficiently modeled using the Morison equation, which accounts for both inertia and drag contributions.

3.3. Structural modeling approaches

According to the fidelity that is required, several methodologies can be used to model the structural behavior of offshore wind turbines. At the highest fidelity level, 3D Finite Element Method (FEM) models can be used for blades, tower and substructure [107–109], with the external loads that can be calculated externally and then applied at each nodes. Despite offering a great accuracy, this method is characterized by very high computational costs, hence when the number or the time of simulations increases, other options are preferred.

To reduce the computational effort, reduced-order structural representations are commonly adopted. An example is represented by 1D beam theories coupled with two-dimensional FEM section analyses performed for the blades in [110], where interesting results are extracted comparing the three different beam models implemented in OpenFAST [111] and the variability induced in the FEM analysis. To further reduce the complexity and increase the computational speed, it is even possible to avoid the FEM section analysis [112,113] limiting the analysis to the blade root, where the stress can be extracted analytically. Such approaches, however, require the adoption of appropriate safety factors to account for the introduced simplifications, as recommended by current standards [114].

Reduced-order beam formulations are also commonly employed for tower modeling. In OpenFAST, for instance, the tower is modeled as a cantilever beam using a modal approach, deriving the first mode shapes using a precomputed FEM, thus limiting the degrees of freedom and the computational effort.

For floating offshore wind turbines, a multibody dynamics formulation is often employed to enable the coupled time-domain simulation of rigid (e.g., substructure) and flexible components (e.g., tower, blades) [96]. OpenFAST adopts Kane's method to efficiently derive the equations of motion of the aero-hydro-servo-elastic system [115]. This approach allows to avoid the explicit introduction of Lagrange multipliers, thus obtaining compact governing equations and improving numerical efficiency. This is particularly useful for long time-domain simulations and large-scale parametric studies. Another formulation of multibody dynamics, the momentum cloud method, is presented in [116]. This methodology is based on the direct application of the conservation of momentum to an entire system, and makes also use prescribed motions between contiguous bodies. The main advantage of using this approach is that an N-body system can be conveniently represented using only six equation of motions, drastically reducing the computational demand. Time-domain solvers relying on lumped-mass representations, such as OrcaFlex [117], are also commonly used to model the coupled structural response of offshore and floating wind systems under combined environmental loading. These tools are particularly suited to analyze large motions and non-linear structural dynamics. A schematic comparison of all the mentioned methodologies is present in Table 4.

3.4. Recent developments in loads calculation

The above sections report the standard frameworks for offshore wind turbine loads evaluation and their strengths and limitations. However, through research and innovation, new theories and technologies are investigated to increase fidelity and reduce the computational costs. An example in the field of aerodynamics is the new 'Unified Momentum Model' [118]. This theory allows to well-predict the behavior of wind turbine forces and power without the empirical corrections required by BEM models for some flow regimes. Additionally, emerging ML techniques are used to accelerate CFD simulations, improve turbulence modeling and reduced-order models [119].

Concerning wave loads, similarly to the wind case, the goal is to increase accuracy while reducing the computational burden. In [120] non-linear kinematics is incorporated to the relative form of Morison's semi-empirical force model to significantly improve the accuracy of rapid simulations. ML frameworks are also used to reduce the use of computational intensive simulations and predict hydrodynamic loads [121]. Regarding the structural side, recent advances are driven by the need to capture increasingly complex non-linear behavior, preserving computational efficiency. Models like the fully non-linear geometrically-exact beam theory are gaining growing attention, since they are able to represent structural coupling and large deflections overcoming the limitations of classical linear beam formulations [122] Moreover, digital twins and data-driven approaches are

Table 4
Qualitative comparison of standard structural modeling approaches for offshore wind turbines.

Method	Core assumptions	Physical behaviors captured	Computational speed	Accuracy
3D FEM	Continuum mechanics; detailed spatial discretization	Stress and strain distribution; local deformation; modal response	+ (hours–days)	+++
Beam + FEM section	1D beam theory; sectional properties from 2D FEM	Global bending and torsion; sectional stiffness effects; modal dynamics	++ (minutes–hours)	++/+++
Simplified beam/blade root models	1D beam theory; analytical stress evaluation;	Global loads; root bending moments; fatigue indicators	+++ (real-time capable)	+
Multibody dynamics (Kane's method)	Rigid and flexible bodies; generalized coordinates; kinematic constraints	Coupled aero-hydro-servo-elastic response; large motions; modal deformation	++ (minutes–hours)	++
Momentum cloud method	System-level momentum balance; prescribed relative motions	Distributed inertia effects; global coupled dynamics	++ (minutes)	++
Lumped-mass solvers (e.g., OrcaFlex)	Lumped-mass approach; non-linear kinematics	Large displacements; non-linear structural response; coupled environmental loading	++ (minutes–hours)	++

increasingly used to evaluate the loads and the damage on the blades and structure. These approaches are discussed among the novelties in the next chapters.

4. Fatigue evaluation methods

Fatigue failure refers to the abrupt fracture of a material resulting from repeated or fluctuating stress cycles applied over time. A distinguishing characteristic of these stresses is that they typically remain below the material's ultimate tensile strength, but they have been repeated or fluctuating a large number of times [123]. Fatigue regimes are often classified according to the number of cycles that precede failure: Low Cycle Fatigue (LCF) if they are below 10^4 cycles, High Cycle Fatigue (HCF) when they are between 10^4 and 10^7 and Very High Cycle Fatigue (VHCF) if they are above 10^7 [124]. Concerning wind turbines, they experience $> 10^7$ random cycles during their average life, therefore they can be inserted in the last section (VHCF). This cyclic loading is related to wind, gravity, and gyroscopic effects, which cause the turbines to be vulnerable to structural failure. Among those, wind load fluctuations are considered the most detrimental for the fatigue life [23].

Fatigue failure is a process structured in several stages: at the beginning, the initiation of microcracks (nucleation) is induced by cyclic plastic deformation, followed by crystallographic propagation from two to five grains. This kind of cracks are not detectable to the naked eye. Later, microcracks become macrocracks, creating parallel plateau like fractures, divided by longitudinal ridges: they are smooth and normal to the direction of the maximum tensile stress. At the next stage, the remaining material is no more able to ensure the resistance to the loads, and this leads to a sudden and rapid fracture that can be ductile, brittle or a combination of both.

Fatigue cracks will typically initiate at discontinuities in the material where the cyclic stress is a maximum and, if other external mechanism are involved in the nucleation phase (e.g., temperature effects like creep, corrosion), damage modeling become even more complex [123,125].

Although fatigue damage is evaluated using similar frameworks for blades, tower, and substructure, differences in material behavior and dominant loading mechanisms must be considered when interpreting load predictions for component-specific design. As described by IEC 61400-1, to calculate the fatigue life of a wind turbine an appropriate fatigue accumulated damage calculation method should be used [30]: the most common is the Miner Rule [126–128], a linear approach, whose main drawback is that it does not take into account the loading history as well as overlooking interaction events [129]. To derive the damage induced by a cyclic loading, S–N curves are often used. S–N curves, also known as Wöhler curves, represent the relationship between the stress range applied to a material and the number of cycles to failure under cyclic loading. The data are typically plotted with the stress range on the vertical axis and the number of cycles (on a logarithmic scale) on the horizontal axis.

Nevertheless, also fracture mechanics can be employed to evaluate fatigue life as support to S–N curves as DNV-RP-C203 suggests. Fracture mechanics is a section of mechanics that investigate the initiation and propagation of cracks in materials. It provides theoretical and quantitative tools to predict failure due to crack growth under various loading conditions. By considering material properties, stress intensity factors, and energy release rates, fracture mechanics is able to assess structural life in the presence of defects or pre-existing flaws. Despite this, since crack initiation is not included in this methodology, a shorter fatigue life is obtained through fracture mechanics than by S–N data [130]. In the next paragraphs, a more detailed description of these two methodologies is presented.

4.1. S-N curves

S–N curves are diagrams that represent the fatigue strength of the material versus the life (expressed as cycles) when subjected to constant stress range loading and fixed stress ratio $R = \sigma_{min}/\sigma_{max}$. These charts are the product of the loading of controlled specimens, hence they do not entirely represent a machine part and require corrections [131]. In order to take into consideration the differences between the controlled specimens and the real components, factors are defined with regard to surface conditions, loading, size and geometry (including stress concentration effects), reliability, temperature and miscellaneous factors [123]. The S–N curves can be derived for both metals and composites, hence they can correlate stresses and allowable load cycles for every material composing wind turbines. The structure of an S–N curve for a metal is reported in Fig. 9 and can be described as follow:

- A diagonal line discovered by Basquin [132], who was the first to approach the fatigue behavior. It is described by the following equation:

$$\sigma = C_1(N)^{C_2} \tag{10}$$

  where C_1 and C_2 are material constants, σ is the stress and N are the cycles to failure.
- A knee that introduces a straight horizontal line, which was discovered by Stromeyer [133], who firstly introduced a truncation of Basquin curve at fatigue limit stress σ_w namely the stress below which the material can ideally undergo an infinite number of cycles.

$$\sigma = \sigma_w + C(10^6/N)^{1/4} \tag{11}$$

  while N is the number of cycles and C is a material constant.

There are also other models of S–N curves, such as Palmgren [134] or Weibull [135]. The common point of all these methodologies is that they are not proper models, but rather data fitting procedures which are dependent on the specimen features [136]. Despite most material see a fatigue limit in the regime of high cycle fatigue, this concept has to be treated carefully, especially in free corrosion conditions or even with variable amplitude loading [137]. In fact, with proper testing, it is possible to highlight that in steel alloys after a first horizontal limit, a second descending curve trend is present, followed by a second fatigue limit at lower stress. This behavior is caused by a second mechanism of crack formation, namely the passage from surface to subsurface crack initiation. An example of the two mechanism is presented in Fig. 10. Concerning aluminum alloys, an ever decreasing stress S–N curve is usually found, even up to 10^{10} cycles [138]. Hence, sufficient testing data is required to correctly evaluate the corresponding remaining cycles. Being derived by specimen related data, the values assumed by S–N curves are highly dependent on the methodology used to fit them. Moreover, it is common to find a huge scatter range even in controlled experiments; this is basically due to the variability of the microstructure and the scatter of defect size, but it can also be caused by poor alignment of specimen and testing machine [136]. For this reason, it is also widespread the use of probabilistic S–N curves [139]: in this way, applied stress and fatigue life are related by iso-probabilistic curves, giving an indication also on the chance of failure. It is possible to choose the among several confidence level of survival and one of the most used is the curve with 97% chance of survival.

Since the curves are evaluated for unloaded material, it is also possible to modify the S–N curve to take into account the damage induced by precedent cycles. The idea behind this procedure is illustrated in Fig. 11: given a stress σ_1 with corresponding cycles to fatigue failure N_1, after a number of cycles n_1 at σ_1, the maximum number of cycles that can be performed again at σ_1 is $N_1 - n_1$; (σ_1, $N_1 - n_1$) is the first point of the new S–N curve. The second point is obtainable knowing the previous fatigue limit σ_0 and its corresponding N_0: after the cycles performed at σ_1 the number of cycles n_0 allowable at σ_0 will be:

$$\frac{n_1}{N_1} + \frac{n_0}{N_0} = 1 \tag{12}$$

hence:

$$n_0 = (N_1 - n_1)\frac{N_0}{N_1} \tag{13}$$

the number of cycles at which the fatigue limit is reached is to be considered as a constant. In this way the new S–N curve is complete. There are also other methodologies to update the curves following the progressive damage: more detailed information can be found in [123]. When it comes to composite materials, the behavior is much more complex due to the inhomogeneities and the anisotropy at the nanometer length scale. This feature is cause of several damage phenomena (e.g., matrix cracking, matrix crazing, fiber fracture and buckling etc.) which inevitably influence the damage behavior [140] and consequently the variability of S–N curves shape (Fig. 12). In [141], composite S–N curve models proposed by Weibull [142], Sendeckyj [143], Kim and Zhang [144] are found to be the best fitting equations for experimental fatigue data obtained by Weibull for R = −1, Sendeckyj for R = 0.1, and Kawai and Itoh for R = −0.43, −3, and 10 [145].

4.2. Miner's rule limitations

As mentioned in the previous paragraph, S–N curves represent the relationship between the cyclic stress range and the number of cycles required for fatigue failure, keeping constant the stress ratio *R*. Hence, when it comes to variable loading, each cycle has to be identified and associated to a certain damage to estimate the fatigue life of the component. To do so, the stress history has to be analyzed and cycles counted. Standards like ASTM E1049-85 [130,147] cite rainflow algorithm and similar among the acceptable methodologies for variable loading cycles counting. In addition to time-domain cycle counting methods, fatigue cycles can be also estimated using frequency-domain

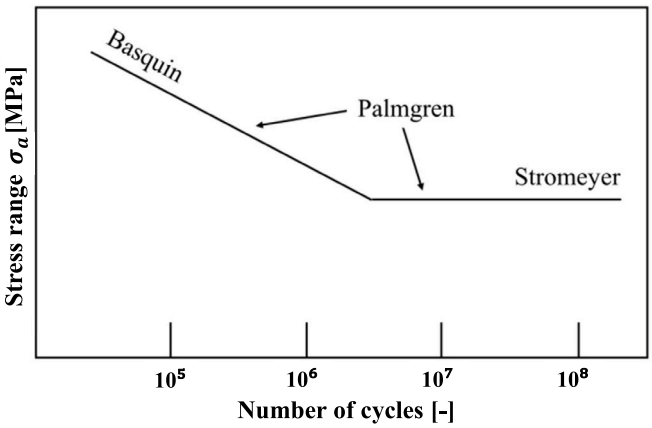

Fig. 9. S–N curve for a metal.
Source: adapted from [136].

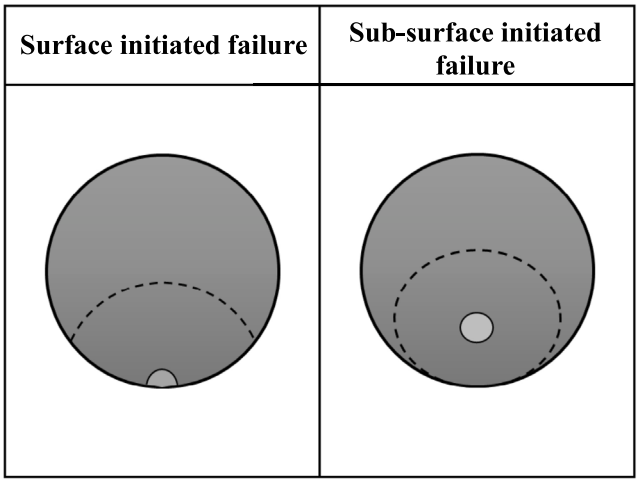

Fig. 10. Crack initiation modes: surface (left), sub-surface (right).
Source: adapted from [146].

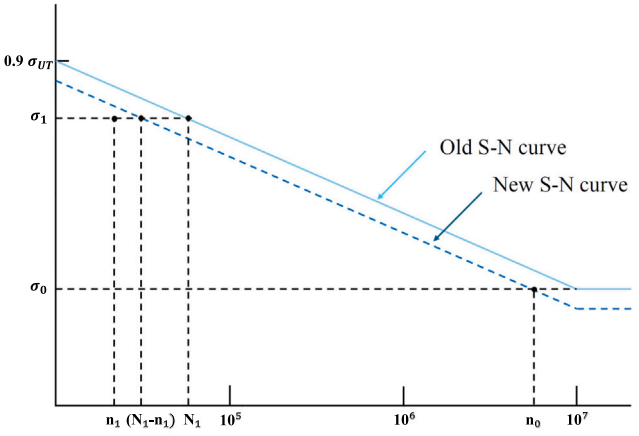

Fig. 11. Example of S–N curves translation for precedent loading.

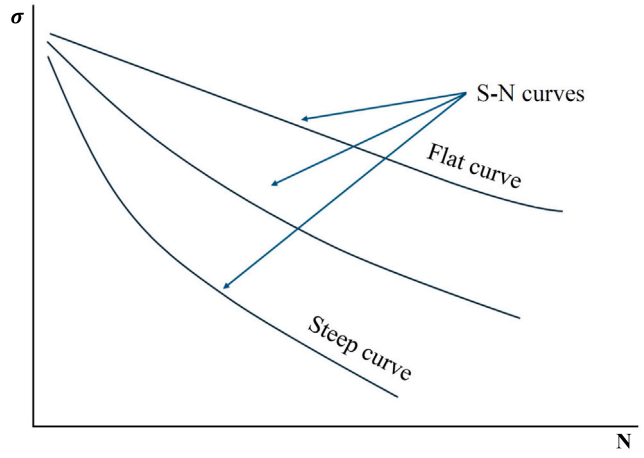

Fig. 12. Example of S–N curves variability for composite materials. *Source:* Adapted from [140].

approaches based on the statistical properties of the stress response. Spectral methods, as the Dirlik formulation [148] and the Benasciutti–Tovo model [149], derive the stress range distribution directly from the power spectral density of the load or stress signal, avoiding the need for long time-history simulations and explicit rainflow counting. These approaches are mostly employed for stationary random loading conditions and offer significant computational advantages for long-term fatigue assessment. After having established the number of cycles, damage accumulation models like Palmgren-Miner rule are used to evaluate the fatigue life of both structure and blades.

$$D = \sum_{i=1}^{n} \frac{1}{N(\sigma_i)} \leq \Delta \tag{14}$$

In the above equation, D is the cumulative fatigue damage, N are the cycles performed at a corresponding fatigue failure stress σ_i while Δ corresponds to the value of cumulative damage associated to failure. Generally, Δ is considered equal to 1, but indeed it is a distribution of values whose mean is equal to one [150]; this feature derives from the intrinsic variability in fatigue strength of the material and adds another source of uncertainty representable through the covariance of the distribution itself. Typical values of the coefficient of variation of Δ (COV_Δ) are 0.3 or 0.45 [24]. Miner's rule is a linear method, widely used because of its simplicity, and also because the accuracy of results obtained using other more complex methodologies is still affected by equal or higher uncertainty. Nonetheless, there are other approaches that try to overcome Miner's rule limitation as the inclusion of the chronological order of loads series, as Mesmacque et al. [151] and also non-linear theories which address the non-linear phenomena excluded in Miner's approach [152]. As an example, in [153,154], new models for the evaluation of cumulative damage are presented, which include load interaction phenomena and also the strength degradation induced by loading history. Nevertheless, to determine the fatigue damage produced by each stress level, S–N curves are used, as they are commonly adopted for high cycle fatigue and gigacycle fatigue [155].

It is also worth mentioning that for wind energy application, fatigue assessment is often performed through the concept of Damage Equivalent Load (DEL). Instead of directly evaluating the damage, variable amplitude loading histories ($\Delta\sigma_i = \sigma_{max,i} - \sigma_{min,i}$ and associated number of cycles n_i) are converted into an equivalent constant-amplitude stress (as shown in Eq. (15)) which induces the same fatigue damage over a predefined number of cycles N_{eq}. This approach is still based on Palmgren-Miner linear accumulation damage and on material S–N curves, hence it involves the same uncertainties discussed above.

$$DEL = \left(\frac{\sum_i n_i (\Delta\sigma_i)^m}{N_{eq}} \right)^{\frac{1}{m}} \tag{15}$$

4.3. Stress concentration factors

When it comes to offshore support structures and platforms, the presence of welded joints leads to local stress hotspots where the real value of the stress can be higher than the nominal one, calculated using simple beam theory and superposition theory. This phenomenon may lead to unexpected crack initiation and fatigue failure and therefore has to be taken into account. To do so, the use of Stress Concentration Factors (SCFs), which are defined as the ratio between the local stress at the welding surface and the nominal stress [156], is recommended by several standards [130,157,158]. The SCF depend on the welding profiles and can be calculated using several methods which can be classified into three groups [159,160] and are resumed in Table 5:

- *Experimental evaluations*: in this methodology, local strain/stresses are measured through strain gauges placed at the weld toe. Nominal stress can be calculated using measurements or analytical solutions.
- *Empirical equations*: it is possible to obtain SCF using the empirical equations given by standards even though they are useful only in case of simple geometry. Among the empirical approaches, [161] is the most used and suggested in standards like [130], because is able to provide SCFs for axial load, in-plane bending, and out-of-plane bending, according to the joint type.
- *Finite Element Analysis (FEA)*: This methodology is able to identify the locations of critical points in addition to the value of local stress.

Moreover, hybrid approaches are present in literature, such as [159]. These methodologies can be useful to overcome some accuracy limitations while keeping the costs and the time still acceptable. Finally, in [162] a comparison is presented among two empirical approaches and FEA, resulting in the latter being less conservative and highlighting the influence of the SCF methodology choice on expected fatigue life.

4.4. Fracture mechanics approach

Although S–N curves are used in many standards for the design of offshore wind turbines, they do not lead to crack growth information (i.e., size of the crack) but can only estimate the cumulative fatigue damage [163]. Hence, besides the importance of good design, in-service inspections as well as maintenance and repair are needed to keep structural safety and system integrity throughout the life of the turbine. This has contributed to the development of fracture mechanics (FM) and reliability-based methods to evaluate crack growth in any structure [164]. As previously mentioned, the fatigue phenomena is divided into three stages: the first one is associated to crack initiation, the second one is related to crack extension and the third one to the rapid acceleration in crack growth with final failure. To evaluate the effect that the stress produces on the crack and its growth, the stress intensity K is introduced [123]:

$$K_1 = \beta\sigma\sqrt{\pi a} \tag{16}$$

where β is the stress intensity modification factor, σ is the nominal stress and a is the characteristic crack length. Similarly, given a stress range associated to a cycle $\Delta\sigma = \sigma_{max} - \sigma_{min}$, it is possible to evaluate the stress intensity range:

$$\Delta K_1 = \beta\Delta\sigma\sqrt{\pi a}. \tag{17}$$

Not every ΔK is associated to crack growth as there is a threshold value generally called ΔK_{th}. Assuming that the crack is in the second stage, namely the crack growth region, its progressive growing can be approximated using the *Paris Equation*:

$$\frac{da}{dN} = C(\Delta K_1)^m \tag{18}$$

Table 5
Qualitative comparison of the three methodologies to model SCF [159].

Method	Accuracy	Time	Limitations
Experimental evaluations	+++	+++	Not always possible to place the gauges close to the weld toe.
Empirical equations	++	+	Only valid for simple geometries, incapable of detecting the location of crack initiation.
Finite Element Analysis	++	++	Inaccuracy in the geometry may lead to significant discrepancies.

where C and m are empirical, tabulated material constants and N is the number of load cycles. By simply integrating the above equation, it is possible to evaluate the growth of the crack until a predefined failure length a_f. In [24] a comprehensive review of the main uncertainties related to fracture mechanics approach is presented. They can be divided into uncertainties related to initiation phase and initial crack size, crack growth rate, stress intensity factor, inspection and repair and crack propagation models.

Concerning the crack initiation phase and the initial crack size, in [165] the Weibull function is used to correlate the mean value of crack size and time. Moreover, the time to crack initiation is considered as proportional to the propagation time, hence it is possible to model both the phases obtaining the crack dimensions throughout the fatigue life. Nevertheless, this approach requires the initial crack length, which is difficult to be estimated. A possible approach to overcome this issue is to use the S–N curves. This methodology consists in estimating the size of the crack in order to reach the same expected fatigue life derived by the S–N curves, as a sort of calibration [166,167]. The process of crack growth has a stochastic nature as well, hence the rate in crack growth contains a statistical variability that is a direct consequence of material properties variability, geometrical tolerances, pre-existing defects and loading conditions [168]. The problem in evaluating these uncertainties is related to the estimation of the constants C and m in Paris law equation, which is the most used to model the fatigue crack growth rate [24]. It is possible to use both experimental methodologies using standard specimens, pre-cracked and notched or even numerical calculation as discussed in [169].

Moving to the stress intensity factors, standard procedure is the use of FEM and theoretical predictions available in literature. Nonetheless other methods are also proposed such as Strong Formulation Finite Element Method (SFEM) in [170] or [171] where the measured crack opening displacement is used coupled with a least-squares method to obtain stress intensity factors. For steel structures the main uncertainty issue is related to the welds geometry, which influences the SCF distribution and the location of the most critical fatigue location [172], hence in addition to the conventional theoretical correlations or finite element methods, also hybrid approaches have been developed as [159].

Finally, also crack propagation modeling options create an uncertainty on the results of fatigue analysis. As previously mentioned, Paris model of crack growth is the most common, nevertheless brings the limitation of not considering the R stress ratio parameter. An example of going beyond these limitation is the Walker Law [173] which addresses this issue for metallic materials by introducing a third parameter γ_w:

$$\frac{da}{dN} = C_W \left[\frac{\Delta K_1}{(1-R)^{1-\gamma_W}}\right]^{m_W} \tag{19}$$

where C_W and m_W are equivalent to the C and m of Paris Law. Note that if γ_W is 0, the crack propagation is not influenced by the stress ratio. For additional and more detailed information, a comprehensive review of crack propagation models for metallic materials is carried out in [174].

Concerning composite materials, the anisotropy and heterogeneity typical of composites generates uncertainty in their crack growth evaluation. A lot of effort has been performed in the recent years, in particular through the use of numerical calculation methods such as the extended Finite Element Methods (XFEM) [175,176], and also other approaches such as peridynamic (PD) based models [177].

In [164] a comparison between fracture mechanics and S–N curve approach is performed for a bottom fixed wind turbine. The results show that the reliability index of the structure calculated at the end of life using the S–N curves is 3.4 times higher than using fracture mechanics. Hence the latter approach is more conservative. This result is confirmed also in [178]. In [179] a comparison of the fatigue damage at the tower base section is performed. The fracture mechanics approach forecasts two times higher damages with respect to the S–N curves in all the locations of the section.

It is important to remark that, in this work and explicitly in the present section, fracture mechanics has been introduced primarily as an extension of fatigue modeling through crack growth laws. However, when pre-existing and detected defects are explicitly considered, fracture mechanics assumes a fundamentally different role within structural integrity assessment. In such cases, fracture assessment is aimed at evaluating the safety and fitness-for-service of offshore wind structures rather than predicting fatigue life. In such cases, fracture assessment aims at evaluating the safety and fitness-for-service of offshore wind structures rather than predicting fatigue life. As an example, the reliability of a structure can be enhanced and updated through a fracture mechanics-based approach coupled with inspection and repair strategies. In [180], a comparison is performed between scenarios involving crack detection followed by repair and detection-only strategies, showing that reliability increases when repair is applied. Nevertheless, crack detection in offshore structures is often based on non-invasive techniques to avoid material damage, which introduces a non-negligible probability of missed detection and associated uncertainty in reliability predictions. Therefore, it is common to define a probability of detection (POD), which is dependent on several variables as the nondestructive evaluation method, human factors, test environment, and defect size. Usually, the 95% confidence curve is plotted against the crack size [181]. To reduce detection-related uncertainties, statistical methodologies have been developed [167,182] and also a DNV standard has been released [114].

4.5. Recent developments in fatigue assessment

Fatigue assessment methodologies are now experiencing a significant influence by the growing interest towards ML approaches. In particular, the most promising seem to be hybrid solutions, which embrace both physical significance and data-driven methodologies [183, 184]. ML models are increasingly used to go beyond the S–N curves and linear damage accumulation, directly using material properties and limited sets of experimental data [185]. Moreover, data-driven approaches can be used to predict crack growth rate, improving computational speed but still obtaining accurate predictions [186]. However, despite their strong potential, the lack of an established regulatory framework currently confines these methodologies mainly to research-oriented studies rather than practical engineering applications. Research is also focusing on the field of digital twins [187,188], which can be used to overcome the gap between the design phase and the operative conditions. Using these tools, structural damage is updated using real data, resulting in lower uncertainties and increasing accuracy of remaining life predictions.

Table 6
Literature review of the most common modeling strategies. CE= Cummins equation, MCM= Momentum Cloud Method, BM= Beam Model, RC= Rainflow Counting, FM= Fracture Mechanics, PSD= Power Spectral Density.

Ref.	Aerodynamics	Hydrodynamics	Load evaluation methodologies	Softwares	Fatigue evaluation methodology	Component
[110]	BEM	CE	1D BMs (comparison) + 2D FEM	OpenFAST, Becas	RC, Miner's rule	Blades
[112]	BEM	CE	Euler–Bernoulli BM (ElastoDyn)	OpenFAST, MLife	RC, Miner's rule	Blades, Tower base
[189]	BEM	Morison/ CE	1D BM	Bladed	RC, Miner's rule	Blades
[190]	BEM	Morison	Non-linear Geom. Exact BM	Loose	RC, Miner's rule	Blades
[191]	BEM	CE	Euler–Bernoulli BM (ElastoDyn)	OpenFAST	RC, Miner's rule/ Linear elastic FM	Substructure welded tubular joints
[192]	BEM	CE	Euler–Bernoulli BM (ElastoDyn)	OpenFAST	RC, Miner's rule	Tower base
[193]	BEM	CE	Euler–Bernoulli BM (ElastoDyn)	OpenFAST	RC, Miner's rule	Tower base
[113]	BEM	CE	Euler–Bernoulli BM (ElastoDyn)	OpenFAST, MLife	RC, Miner's rule	Blades, Tower base
[194]	/	/	Strain measurements	/	RC, Miner's rule	Tower base
[195]	BEM	CE	Euler–Bernoulli BM (ElastoDyn), Non-linear Geom. Exact BM (BeamDyn)	Floris, OpenFAST	RC, Miner's rule	Blades, Tower base
[196]	BEM	CE	Euler–Bernoulli BM (ElastoDyn)	OpenFAST	FM	Monopile
[179]	BEM	CE	Euler–Bernoulli BM (ElastoDyn)	OpenFAST	S–N curves/ FM	Monopile
[197]	/	/	Strain measurements	/	RC, Miner's rule	Tower base
[198]	Drag-based	Morison	3D FEM	Fe-safe, ABAQUS	PSD + Miner's rule	Monopile, Tower
[199]	BEM	Morison	1D BM (BeamDyn, SubDyn)	OpenFAST	PSD + Miner's rule	Jacket

5. Discussion

In this article, a review of the uncertainties in the possible approaches and theories to model the fatigue life of an offshore wind turbine has been performed.

In the climatological section, the uncertainties related to the wind evaluation have been discussed, showing that fatigue damage is sensitive to the adopted turbulence model and that approaches involving also low frequency wind cycles lead to lower fatigue life estimations. Among those factors it appears that more priority should be given to the investigation of turbulence. In [200] a comparison of IEC 61400-1 prescriptions on turbulence and wind shear and a model based on wind measurements with full wind, characteristic turbulence intensity and wind shear shows that the standard overestimates of 7.5% the equivalent fatigue loads, with relatively small impact of the wind shear. Standard turbulence models like Mann's and Kaimal's do not account for non-Gaussian effects and other phenomena like wakes generated by nearby turbines, which can affect the turbulence intensity and the calculations with a variability of 5%–15% of turbine loads [201]. However it is still not possible to identify a single turbulence model that universally best represents the atmospheric conditions of a site and to generalize its impact on the loads [202]. In fact, each site may be better or worse characterized by different spectral formulations depending on its specific meteorological and environmental features.

Concerning the wave data and modeling, satellite data and reanalysis models offer an acceptable accuracy at low cost with error estimations on the order of 7% and 10% with respect to the in situ measurements error which are around 6% [203]. The main issue of using satellite data is the revisit time, while in situ campaigns provide the highest accuracy but at high cost and suffering reliability issues. Given the marginal difference in accuracy and in accordance with standard guidelines, both the model and satellite-derived data can be considered sufficiently accurate for fatigue life estimation, provided that appropriate safety factors are applied. Moreover, the importance of spectrum choice, as well as its parameters' tuning has been highlighted, showing their strict dependency on the location features and directly influencing the consistency of fatigue analysis. In [204] the JONSWAP spectrum leads to a shear force root mean square (RMS) value at the mudline around 3% higher than the one calculated using the measured wave spectrum. In the same study, additional comparisons are performed in other locations using JONSWAP and swell-dominant wave spectra, reaching up to 40% variability in the shear force RMS. This highlights the importance of spectrum choice and tuning according to the local wave climate. Some studies have also investigated the influence of sea currents, showing higher fatigue damage for opposite waves-currents. However, their influence according the standards is trivial with respect to the above-mentioned factors.

Additional climatic uncertainties have also been discussed: the climate change context influences the reliability of historical data to forecast future wind and wave distributions. Hence, fatigue damage estimation is also affected, since several world areas are experiencing reduction or increase for both the resources. Nevertheless, it is difficult to provide a quantitative range of uncertainty given the high output variability of those forecasts. Concerning the novelties related to the climatological section, non-gaussian turbulence models are now explored to account for extreme weather conditions while machine learning and data-driven approaches are becoming ever more used, especially for compensating lack of data or reproducing ad-hoc local spectra. However, a standard framework is still missing, hence their application is confined to complementary or research analyses.

In the load evaluation section, aerodynamic loads modeling has been discussed: the most common approach is the BEM theory, which allows good reliability at an affordable computational costs. This methodology is used for aerodynamic calculations in several softwares like OpenFAST, the most common aero-hydro-servo-elastic software used for offshore wind turbine simulations. Some corrections are often implemented to increase accuracy. A comparison between BEM codes and FVWM in [205] shows that BEM codes overestimates the lifetime damage equivalent loads (DELs) of 9%. CFD represents the most accurate modeling strategy, however tends to be avoided in long term fatigue analysis, due to its computational burden and its role is often limited to validation.

For the hydrodynamic loads modeling, linear potential flow theory is usually adopted and Boundary Element method-based solvers are used to extract hydrodynamic coefficients. This methodology is used in several long term fatigue approaches (see Table 6) and can be also integrated with non-linear methodologies (i.e.,CFD) to increase its accuracy. The use of non-linear methodologies is also investigated in literature. In [206] the influence of second order waves leads in an increase of bending moments at the foundation up to 7.5% with respect to linear waves. In [207], the opposite is found for a floating wind turbine tower, where bending moments simulated adopting fully non-linear waves are lower. Nevertheless, for long term fatigue estimations, non-linear methodologies are usually avoided to reduce the computational

burden, providing that appropriate safety factors are used. The effect of multidirectionality and wind-wave misalignment influence is instead less investigated. Despite this, reduction in the loads up to 40/60% is possible as per [64].

As seen in the previous chapters, also the structural model plays a crucial role in the accuracy of fatigue life estimation. High fidelity 3D FEM models provide the most accurate evaluation of local stress field in offshore wind turbines. However, their computational cost hinders their coupling with long-term aero-servo-hydro-elastic simulations. Two main strategies can be adopted to overcome this issue. The first one consists in using the 3D FEM models, calculating the external loads adopting frequency-domain wind and wave analyses. This methodology allows for detailed local fatigue assessment but it is not able to account for coupling effects. The second one, which represent the state of the art of the engineering framework, is to rely on time-domain aero-servo-hydro-elastic simulations based on reduced-order beam type structural models, at the expense of local stress resolution. In [208] a comparison between these two strategies leads to differences in bending moments estimations of 5%–15%. Moreover, in [209] a comparison among a beam model for the blade and its finite element representation shows only 5% difference, showing the validity of both the approaches. Beside the comparison of standardized frameworks, new load evaluation methodologies have been reported, like the 'Unified Momentum Model' for aerodynamics or the 'non-linear geometrically-exact beam theory' for the structural analysis. Together with machine learning techniques, all these strategies aim to reduce computational burden while preserving accuracy.

Finally, in the section related to fatigue evaluation methodologies, the possible approaches to model the process of fatigue damage have been discussed. S–N curves tend to underestimate the fatigue damage with respect to fracture mechanics, with fatigue life estimations that can be two times higher. For both steel based components (i.e, substructures, tower) and composite materials (blades) S–N curves are usually employed for the sake of long term fatigue evaluation. Safety factors are also applied to the stress values used to enter the curves in order to take into account possible load underestimations, additional uncertainties and the statistical variability of the phenomenon. Stress concentration factors should be also used for particular geometries or weldings, which locally increase the load. To extract the fatigue damage, the use of S–N curves is coupled to damage accumulation methods: linear methodologies (e.g., Miner's rule) are preferred since non-linear ones do not add significant confidence to the analysis. Miner's rule is associated to uncertainties in failure between 30%–60% as per [24].

Fatigue life can also be evaluated through fracture mechanics. Nevertheless, several uncertainties are present, which are directly correlated to the stochastic nature of the process and are challenging to estimate. In particular, the evaluation of Paris law equation parameters is not trivial. Another important issue is related to inaccuracy induced by the estimation of initial crack dimension: usually, S–N curves calibration is adopted to obtain the initial crack dimension.

Regarding the recent developments in fatigue, machine learning techniques are explored to overcome the limitations related to S–N curves and linear accumulation models as well as improve the prediction of crack growth rate. As previously discussed, in absence of a regulatory framework, this methodologies are confined to innovation rather than standard engineering practice. Research is also focusing on digital twins, to reduce the gap between design phase and real operative conditions.

6. Conclusion

This review has examined the main engineering methodologies currently adopted for fatigue assessment of large offshore wind turbines, with a focus on the balance between modeling accuracy and computational efficiency. The analysis proves that no single approach is universally optimal, and that model choice must be driven by the aim of the study.

Concerning preliminary design stages, broad parametric analyses, and large-scale optimization tasks, frequency-domain load estimation based on simplified aerodynamic and hydrodynamic theories (e.g., BEM, linear potential flow, and Morison-based formulations) provides an effective compromise between accuracy and computational cost. If combined with FEMs, these approaches enable stress-oriented evaluations while maintaining computational feasibility. Further simplifications through beam-type structural models offer additional reductions in computational effort when local stress resolution is not required.

On the other hand, for detailed investigations of few configurations and especially for floating offshore wind turbines, fully coupled time-domain aero-hydro-servo-elastic simulations represent the current state of the art. These models are essential to capture the non-linear interaction between wind, waves, and structural dynamics, which strongly governs fatigue accumulation. State-of-the-art tools rely on beam-based structural representations coupled with aerodynamic and hydrodynamic solvers, and can be complemented by high-fidelity finite element submodels for localized stress and hotspot fatigue analyses in design phase. Concerning fatigue assessment, the combination of S–N curves and Miner's rule continues to represent the most convenient and established methodology. This is largely driven by its consistency with fracture mechanics approaches, in which crack growth parameters are typically identified by enforcing equivalence with the damage predicted through S–N-based fatigue models.

Future developments in fatigue modeling are expected to be driven by three key directions. First, improved representations of wind and wave excitation, including non-Gaussian turbulence models and refined wave spectra, are required to account for the increasing relevance of extreme environmental events under climate change conditions and local climatological features. Second, machine learning techniques are likely to play a central role in reducing data gaps and enhancing load reconstruction from limited measurements, although their integration into engineering practice will require robust validation and standardization. Third, digital twin frameworks provide a promising pathway towards continuous, data-driven fatigue life updating, narrowing the gap between design assumptions and operational behavior.

Overall, the advancement of offshore wind turbine fatigue assessment will depend on the integration of the above-mentioned novelties (especially data-driven techniques) within unified engineering frameworks, enabling more reliable and efficient predictions of structural integrity over the turbine lifetime.

CRediT authorship contribution statement

Gabriele Mangia: Writing – original draft, Writing – review & editing, Methodology, Investigation, Data curation, Conceptualization, Visualization. **Michele Martini:** Writing – review & editing, Methodology, Investigation, Data curation, Conceptualization. **Giuseppe Giorgi:** Writing – review & editing, Methodology, Conceptualization, Visualization. **Giovanni Bracco:** Writing – review & editing, Supervision, Project administration, Funding acquisition.

Declaration of competing interest

The authors declare that they have no known competing financial interests or personal relationships that could have appeared to influence the work reported in this paper.

Acknowledgments & funding

This publication is part of the project PNRR-NGEU which has received funding from the MUR – DM 117/2023.

Finanziato dall'Unione europea NextGenerationEU | Ministero dell'Università e della Ricerca | Italiadomani

Table A.1
Summary of commonly adopted wind spectra and turbulence models and their treatment in design standards.

Spectrum/model	Equation (compact form)	Standards/typical use
Kaimal (1D)	$S_k(f) = \dfrac{4\sigma_k^2 L_k/V_{\text{hub}}}{\left(1+6fL_k/V_{\text{hub}}\right)^{5/3}}$	IEC 61400-1: wind turbulence spectrum, commonly combined with exponential coherence [30]
Mann (3D→1D equiv.)	$\dfrac{f\,S_i(f)}{\sigma_i^2} = \dfrac{\sigma_{\text{iso}}^2}{\sigma_i^2}\dfrac{4\pi\ell f}{V_{\text{hub}}}\Psi_{ii}\left(\dfrac{2\pi\ell f}{V_{\text{hub}}}\right)$	IEC 61400-1: the 3D field is commonly represented through equivalent 1D component spectra derived from the Mann formulation [30]
Ochi–Shin	$\dfrac{f\,S(f)}{u_*^2} = \begin{cases} 583\,f_*, & f_* \le 0.003 \\ \dfrac{420\,f_*^{0.7}}{(1+f_*^{0.35})^{11.5}}, & 0.003 < f_* \le 0.1 \\ \dfrac{838\,f_*}{(1+f_*^{0.35})^{11.5}}, & f_* > 0.1 \end{cases}$	DNV-RP-C205: empirical offshore wind spectrum with enhanced low-frequency energy content (but less than Frøya), particularly suited for offshore ambient wind conditions [35].
Simiu and Leigh	$\dfrac{f\,S(f)}{u_*^2} = \begin{cases} a_1 f_* + b_1 f_*^2 + d_1 f_*^3, & f_* \le f_m, \\ c_2 + a_2 f_* + b_2 f_*^2, & f_m < f_* \le f_s, \\ 0.26\,f_*^{-2/3}, & f_* > f_s, \end{cases}$	DNV-RP-C205: empirical wind spectrum proposed by Simiu and Leigh; it is developed accounting for wind energy in low frequency range [35].
Frøya	$S_u(f) = 320\left(\dfrac{U_0}{10}\right)^2\left(\dfrac{z}{10}\right)^{0.45}\left(1+\tilde{f}^n\right)^{-5/(3n)}$, $\tilde{f} = 172\,f\left(\dfrac{z}{10}\right)^{2/3}\left(\dfrac{U_0}{10}\right)^{-0.75}$	DNV-RP-C205: offshore wind spectrum calibrated for North Sea conditions, commonly used when low-frequency range is of importance [35]

Appendix. Commonly adopted short-term wind spectra and turbulence representations in design standards

Table A.1 summarizes the most commonly adopted short-term wind spectra and equivalent one-dimensional turbulence representations, used in wind engineering design standards and guidelines.

In Kaimal spectrum: f [Hz] is the frequency, k refers to the velocity component direction (i.e. 1,2,3), S_k is the single-sided velocity component spectrum, σ_k is the velocity component standard deviation, L_k is the velocity component integral scale parameter. V_{hub} is the hub height mean wind speed.

In the one-sided spectra derived from Mann's turbulence model: f [Hz] is the frequency, i refers to the velocity component direction (i.e. 1,2,3), S_i is the single-sided velocity component spectrum, σ_i^2 is the velocity component variance, σ_{iso}^2 is the unsheared, isotropic variance, l is the scale parameter, Ψ_{ii} is the one-dimensional, wave number autospectrum. V_{hub} is the hub height mean wind speed.

In Ochi-Shin:

$$f_* = \frac{f \cdot z}{U_{10}(z)} \tag{A.1}$$

where f is the frequency [Hz], U_{10} is the 10-minute mean wind speed at height z above the sea surface. u^* represents the frictional velocity.

In Simiu and Leigh, f_* is the same as Eq. (A.1). In addition:

$$a_1 = \frac{4L_u\beta}{z}, \tag{A.2}$$

$$\beta_1 = 0.26\,f_s^{-2/3}, \tag{A.3}$$

$$b_2 = \frac{\frac{1}{3}a_1 f_m + \left(\frac{7}{3} + \ln\frac{f_s}{f_m}\right)\beta_1 - \beta}{\frac{5}{6}(f_m - f_s)^2 + \frac{1}{2}(f_m^2 - f_s^2) + 2f_m(f_s - f_m) + f_s(f_s - 2f_m)\ln\frac{f_s}{f_m}}, \tag{A.4}$$

$$a_2 = -2b_2 f_m, \tag{A.5}$$

$$d_1 = \frac{2}{f_m^3}\left(\frac{a_1 f_m}{2} - \beta_1 + b_2(f_m - f_s)^2\right), \tag{A.6}$$

$$b_1 = -\frac{a_1}{2f_m} - 1.5\,f_m d_1, \tag{A.7}$$

$$c_2 = \beta_1 - a_2 f_s - b_2 f_s^2, \tag{A.8}$$

$$\beta = \frac{\sigma_u^2}{u_*^2} = 6.0. \tag{A.9}$$

Furthermore, f_m is the dimensionless frequency at which $fS(f)$ is maximum, f_s is the dimensionless frequency corresponding to the lower bound of the inertial subrange, L_u is the integral length scale and σ_u is the standard deviation of the wind speed. In Frøya spectrum: U_0 is the 1-hour mean wind speed at 10 m height [m/s] and z is the height above sea [m], $n = 0.468$ and f is the frequency [Hz]. Additional information may be found directly in the standards [30,35].

References

[1] United Nations, URL https://www.un.org/en/climatechange/paris-agreement. (Accessed 10 July 2024).
[2] IEA, URL https://www.iea.org/data-and-statistics/data-tools/greenhouse-gas-emissions-from-energy-data-explorer. (Accessed 10 July 2024).
[3] IEA, URL https://www.iea.org/reports/net-zero-by-2050. (Accessed 11 July 2024).
[4] H. Ritchie, P. Rosado, Our World in Data (2020) https://ourworldindata.org/electricity-mix.
[5] M.O. Siddiqui, P.R. Feja, P. Borowski, H. Kyling, A.R. Nejad, J. Wenske, Renew. Sustain. Energy Rev. 188 (2023) 113767.
[6] M.D. Esteban, J.J. Diez, J.S. López, V. Negro, Renew. Energy 36 (2) (2011) 444–450.
[7] S. Hong, J. McMorland, H. Zhang, M. Collu, K.H. Halse, Ocean Eng. 304 (2024) 117793.
[8] F. Zahle, T. Barlas, K. Lonbaek, P. Bortolotti, D. Zalkind, L. Wang, C. Labuschagne, L. Sethuraman, G. Barter, Definition of the IEA Wind 22-Megawatt Offshore Reference Wind Turbine, Tech. Rep., National Renewable Energy Laboratory (NREL), Golden, CO (United States), 2024.
[9] HDblog.it, URL HDblog.it. (Accessed 11 September 2024).
[10] A. Buljan, URL https://www.offshorewind.biz/2024/06/10/18-mw-offshore-wind-turbine-installed-at-test-site-in-china/. (Accessed 11 September 2024).
[11] Offshore, URL https://www.offshore-mag.com/renewable-energy/news/55294623/dongfang-electric-company-china-tests-worlds-largest-offshore-wind-turbine. (Accessed 14 January 2026).
[12] O. Al-Khudairi, H. Hadavinia, C. Little, G. Gillmore, P. Greaves, K. Dyer, Materials 10 (10) (2017) 1152.
[13] J. Velarde, E.E. Bachynski, Energy Procedia 137 (2017) 3–13.
[14] S.H. Sørum, G. Katsikogiannis, E.E. Bachynski-Polić, J. Amdahl, A.M. Page, R.T. Klinkvort, Wind Energy 25 (10) (2022) 1684–1709.
[15] L. Chen, B. Basu, Wind Energy 22 (2) (2019) 327–339.
[16] J. Dai, W. Hu, X. Yang, S. Yang, Ocean Eng. 159 (2018) 187–200.

[17] Y. Yang, M. Bashir, J. Wang, C. Michailides, S. Loughney, M. Armin, S. Hernández, J. Urbano, C. Li, Ocean Eng. 217 (2020) 107909.
[18] U. Bhardwaj, A. Teixeira, C.G. Soares, Renew. Energy 141 (2019) 693–706.
[19] S. Mozafari, P. Veers, J. Rinker, K. Dykes, Wind Energy Sci. 9 (4) (2024) 799–820.
[20] H.S. Toft, L. Svenningsen, J.D. Sørensen, W. Moser, M.L. Thøgersen, Renew. Energy 90 (2016) 352–361.
[21] S.C. Warder, M.D. Piggott, Appl. Energy 380 (2025) 124956.
[22] M. Ramezani, D.-E. Choe, K. Heydarpour, B. Koo, Renew. Sustain. Energy Rev. 185 (2023) 113610.
[23] D. Liao, S.-P. Zhu, J.A. Correia, A.M. De Jesus, M. Veljkovic, F. Berto, Renew. Energy 200 (2022) 724–742.
[24] Y. Dong, Y. Garbatov, C.G. Soares, Ocean Eng. 264 (2022) 112514.
[25] I. Van der Hoven, J. Atmos. Sci. 14 (2) (1957) 160–164.
[26] F. Vorpahl, H. Schwarze, T. Fischer, M. Seidel, J. Jonkman, Wiley Interdiscip. Rev. Energy Environ. 2 (5) (2013) 548–570.
[27] W. Rex, Output-Only Aeroelastic Analysis of Helicopters in Atmospheric Turbulence (Ph.D. thesis), Technische Universität München, 2021.
[28] J.P. Murcia, P.-E. Réthoré, N. Dimitrov, A. Natarajan, J.D. Sørensen, P. Graf, T. Kim, Renew. Energy 119 (2018) 910–922.
[29] J. Pacheco, F. Pimenta, S. Guimarães, G. Castro, Á. Cunha, J.C. Matos, F. Magalhães, Eng. Struct. 300 (2024) 117140.
[30] IEC 61400-1: Wind Energy Generation Systems Design Requirements, International Electrotechnical Commission, 2019.
[31] DNVGL-ST-0437: Load and Site Conditions for Wind Turbines, Det Norske Veritas, 2016.
[32] J. Mann, J. Fluid Mech. 273 (1994) 141–168.
[33] J.C. Kaimal, J. Wyngaard, Y. Izumi, O. Coté, Q. J. R. Meteorol. Soc. 98 (417) (1972) 563–589.
[34] L. Dong, W.H. Lio, E. Simley, Wind Energy Sci. 6 (6) (2021) 1491–1500.
[35] DNV-RP-C205: Environmental Conditions and Environmental Loads, Det Norske Veritas, 2014.
[36] L. Arany, S. Bhattacharya, J. Macdonald, S.J. Hogan, Wind Energy 18 (12) (2015) 2171–2197.
[37] M. Borunda, K. Rodríguez-Vázquez, R. Garduno-Ramirez, J. de la Cruz-Soto, J. Antunez-Estrada, O.A. Jaramillo, Energies 13 (8) (2020) http://dx.doi.org/10.3390/en13081885, URL https://www.mdpi.com/1996-1073/13/8/1885.
[38] W. Weibull, J. Appl. Mech. (1951).
[39] A. Peña, C.B. Hasager, J. Lange, J. Anger, M. Badger, F. Bingöl, O. Bischoff, J.-P. Cariou, F. Dunne, S. Emeis, et al., Remote Sensing for Wind Energy, DTU Wind Energy, 2013.
[40] C.B. Hasager, Wiley Interdiscip. Rev. Energy Environ. 3 (6) (2014) 594–603.
[41] P. Potisomporn, T.A. Adcock, C.R. Vogel, Energy Rep. 10 (2023) 4781–4790.
[42] M. Qin, W. Shi, W. Chai, X. Fu, L. Li, X. Li, Renew. Energy 208 (2023) 450–464.
[43] S. Dai, T. Shi, H. Wang, S. Tang, Y. Song, Y. Liang, J. Wen, ISOPE International Ocean and Polar Engineering Conference, ISOPE, 2024, p. ISOPE–I.
[44] N. Sadeghi, P. D'Antuono, N. Noppe, K. Robbelein, W. Weijtjens, C. Devriendt, Wind Energy Sci. Discuss. 2023 (2023) 1–20.
[45] N. Sadeghi, K. Robbelein, P. D'Antuono, N. Noppe, W. Weijtjens, C. Devriendt, J. Phys.: Conf. Ser., 2265 (3) (2022) 032063.
[46] G. Marsh, C. Wignall, P.R. Thies, N. Barltrop, A. Incecik, V. Venugopal, L. Johanning, Int. J. Fatigue 82 (2016) 757–765.
[47] J. Knight, C. Obhrai, IOP Conf. Ser.: Mater. Sci. Eng. 700 (1) (2019) 012005.
[48] J. Højstrup, Bound.-Layer Meteorol. 21 (3) (1981) 341–356.
[49] T. Shi, S. Dai, S. Tang, H. Wang, Y. Song, J.-F. Wen, Ocean Eng. 341 (2025) 122532.
[50] H. Liu, R. Yang, Adv. Wind Eng. (2025) 100055.
[51] F. Houndekindo, T.B. Ouarda, Energy Convers. Manage. 327 (2025) 119555.
[52] G.B. Airy, Tides and Waves: Extracted from the Encyclopaedia Metropolitana, Tom. V, 1845, pp. 241–396.
[53] K. Rawson, E. Tupper, in: K. Rawson, E. Tupper (Eds.), Basic Ship Theory (Fifth Edition), fifth ed., Butterworth-Heinemann, Oxford, 2001, pp. 302–364, http://dx.doi.org/10.1016/B978-075065398-5/50012-1, URL https://www.sciencedirect.com/science/article/pii/B9780750653985500121.
[54] W.J. Pierson Jr., L. Moskowitz, J. Geophys. Res. 69 (24) (1964) 5181–5190.
[55] K. Hasselmann, T.P. Barnett, E. Bouws, H. Carlson, D.E. Cartwright, K. Enke, J. Ewing, A. Gienapp, D. Hasselmann, P. Kruseman, et al., Ergaenz. Deutschen Hydrogr. Z., Reihe A (1973).
[56] N. Faedo, Optimal Control and Model Reduction for Wave Energy Systems: A Moment-Based Approach (Ph.D. thesis), Maynooth University, 2020.
[57] U.-J. Lee, W.-M. Jeong, H.-Y. Cho, J. Mar. Sci. Eng. 10 (5) (2022) 578.
[58] M.K. Ochi, E.N. Hubble, Coastal Engineering 1976, 1976, pp. 301–328.
[59] K. Torsethaugen, S. Haver, ISOPE International Ocean and Polar Engineering Conference, ISOPE, 2004, p. ISOPE–I.
[60] G. Cervelli, B. Battisti, G. Mattiazzo, Front. Energy Res. 10 (2022) 908529.
[61] T. Duarte, S. Gueydon, J. Jonkman, A. Sarmento, International Conference on Offshore Mechanics and Arctic Engineering, vol. 45547, American Society of Mechanical Engineers, 2014, p. V09BT09A023.
[62] I. Young, Appl. Ocean Res. 16 (5) (1994) 283–294.
[63] Y. Goda, Coast. Eng. J. 41 (1) (1999) 1–20.
[64] J. Vugts, Appl. Ocean Res. 27 (3) (2005) 173–185.
[65] F. Islek, Y. Yuksel, C. Sahin, H.A.A. Guner, Dyn. Atmos. Oceans 94 (2021) 101165.
[66] European Centre for Medium-Range Weather Forecasts, URL https://www.ecmwf.int/en/forecasts/dataset/ecmwf-reanalysis-v5. (Accessed 10 October 2024).
[67] W. Zhang, H. Zhao, G. Chen, J. Yang, Ocean Eng. 285 (2023) 115295.
[68] J. Liu, B. Li, W. Chen, J. Li, J. Yan, Atmosphere 13 (6) (2022) 935.
[69] Q. Liu, T. Lewis, Y. Zhang, W. Sheng, Int. J. Mar. Energy 12 (2015) 63–76.
[70] S.S. Kolukula, P. Murty, Results Eng. 26 (2025) 104708.
[71] E. Roome, D. Christie, S. Neill, Appl. Ocean Res. 153 (2024) 104282.
[72] U.D. Nielsen, M. Mittendorf, Y. Shao, G. Storhaug, Mar. Struct. 91 (2023) 103470.
[73] J.M. Peeringa, J. Phys.: Conf. Ser. 524 (1) (2014) 012093.
[74] D. Carvalho, A. Rocha, X. Costoya, M. DeCastro, M. Gómez-Gesteira, Renew. Sustain. Energy Rev. 151 (2021) 111594.
[75] R. Davy, N. Gnatiuk, L. Pettersson, L. Bobylev, Renew. Sustain. Energy Rev. 81 (2018) 1652–1659.
[76] A. Martinez, G. Iglesias, Energy Convers. Manage. 234 (2021) 113961.
[77] S.H. Li, Atmos. Res. 288 (2023) 106722.
[78] L. Chen, Renew. Energy 153 (2020) 1428–1438.
[79] Y. Yao, G.H. Huang, Q. Lin, Environ. Syst. Res. 1 (2012) 1–11.
[80] D. Wilkie, C. Galasso, Renew. Sustain. Energy Rev. 134 (2020) 110323.
[81] J. He, Q. Li, P. Chan, X. Zhao, Appl. Energy 329 (2023) 120290.
[82] Riahi, et al., The Shared Socioeconomic Pathways and Their Energy, Land Use, and Greenhouse Gas Emissions Implications: An Overview, Global Environmental Change (2022), Our World in Data, 2017.
[83] R.P. Allan, P.A. Arias, S. Berger, J.G. Canadell, C. Cassou, D. Chen, A. Cherchi, S.L. Connors, E. Coppola, F.A. Cruz, et al., Climate Change 2021: The Physical Science Basis. Contribution of Working Group I To the Sixth Assessment Report of the Intergovernmental Panel on Climate Change, Cambridge University Press, 2023, pp. 3–32.
[84] A. El Yaakoubi, A. Bouzem, R. El Alami, N. Chaibi, O. Bendaou, Ocean Eng. 278 (2023) 114070.
[85] J. Wang, F. Golnary, S. Li, A.U. Weerasuriya, K.T. Tse, Ocean Eng. 311 (2024) 118806.
[86] W. Zhang, J. Calderon-Sanchez, D. Duque, A. Souto-Iglesias, Appl. Ocean Res. 150 (2024) 104075.
[87] M.O.L. Hansen, J.N.r. Sørensen, S. Voutsinas, N. Sørensen, H.A. Madsen, Prog. Aerosp. Sci. 42 (4) (2006) 285–330.
[88] Z. Sun, J. Chen, W.Z. Shen, W.J. Zhu, Renew. Energy 96 (2016) 824–831.
[89] U. Boatto, P.A. Bonnet, F. Avallone, D. Ragni, Renew. Energy 214 (2023) 307–317.
[90] F. Papi, J. Jonkman, A. Robertson, A. Bianchini, Wind Energy Sci. Discuss. 2023 (2023) 1–29.
[91] X. Wang, C. Cai, S.-G. Cai, T. Wang, Z. Wang, J. Song, X. Rong, et al., Renew. Sustain. Energy Rev. 175 (2023) 113144.
[92] K. Shaler, E. Branlard, A. Platt, J. Jonkman, J. Phys.: Conf. Ser. 1452 (1) (2020) 012064.
[93] Z. Chen, X. Wang, Y. Guo, S. Kang, Renew. Energy 163 (2021) 1849–1870.
[94] K. Shaler, B. Anderson, L.A. Martínez-Tossas, E. Branlard, N. Johnson, Wind Energy Sci. 8 (3) (2023) 383–399.
[95] L. Greco, C. Testa, Renew. Energy 164 (2021) 444–459.
[96] E. Faraggiana, G. Giorgi, M. Sirigu, A. Ghigo, G. Bracco, G. Mattiazzo, J. Ocean Eng. Mar. Energy 8 (3) (2022) 433–456.
[97] Ansys, URL https://www.ansys.com/products/structures/ansys-mechanical#tab1-2. (Accessed 5 November 2024).
[98] Wamit Inc, URL https://www.wamit.com/. (Accessed 5 November 2024).
[99] R. Kurnia, G. Ducrozet, Comput. Phys. Comm. 292 (2023) 108885.
[100] I. Zabala, J. Henriques, T. Kelly, P. Ricci, J. Blanco, Ocean Eng. 295 (2024) 116913.
[101] G. Giorgi, M. Penalba, J. Ringwood, Nonlinear hydrodynamic models for heaving buoy wave energy converters, 2016.
[102] B.W. Schubert, W.S. Robertson, B.S. Cazzolato, M.H. Ghayesh, Ocean Eng. 197 (2020) 106828.
[103] G. Giorgi, S. Sirigu, M. Bonfanti, G. Bracco, G. Mattiazzo, J. Ocean Eng. Mar. Energy 7 (4) (2021) 439–457.
[104] M. Penalba, G. Giorgi, J.V. Ringwood, Renew. Sustain. Energy Rev. 78 (2017) 1188–1207.
[105] M.A. Bhinder, A. Babarit, L. Gentaz, P. Ferrant, Proceedings of the 9th European Wave and Tidal Energy Conference, Southampton, UK, 2011, pp. 5–9.
[106] Y. Zhang, H. Xu, Y. Law, H. Santo, A. Magee, Ocean Eng. 287 (2023) 115701.
[107] P.A. Kulkarni, A.S. Dhoble, P.M. Padole, Proc. Inst. Mech. Eng. C: J. Mech. Eng. Sci. 233 (8) (2019) 2794–2812.
[108] A. Campos, C. Molins, P. Trubat, D. Alarcón, Energy Procedia 137 (2017) 177–185.
[109] C.L. Bottasso, F. Campagnolo, A. Croce, S. Dilli, F. Gualdoni, M.B. Nielsen, Multibody Syst. Dyn. 32 (2014) 87–116.
[110] M. Sirigu, S. Gigliotti, D. Issoglio, G. Giorgi, G. Bracco, Heliyon 10 (4) (2024).
[111] J. Jonkman, M. Sprague, URL: https://openfast.readthedocs.io/en/main.
[112] M. Ucar, M. Hmedi, E. Uzunoglu, E. Oguz, Ocean Eng. 330 (2025) 121101.

[113] A. Ulazia, H. Ezpeleta, G. Ibarra-Berastegi, J. Sáenz, N. Martinez-Iturricastillo, J.V. Ringwood, Ocean Eng. 299 (2024) 117424.
[114] DNV, G.L., DNVGL-RP-C210 Probabilistic Methods for Planning of Inspection for Fatigue Cracks in Offshore Structures, DNL GL Standard, Oslo, Norway, 2015.
[115] T.R. Kane, D.A. Levinson, Dynamics, Theory and Applications, McGraw Hill, 1985.
[116] B. Sweetman, L. Wang, J. Eng. Mech. 140 (2) (2014) 257–267.
[117] Orcina, URL https://www.orcina.com/orcaflex/. (Accessed 23 January 2026).
[118] J. Liew, K.S. Heck, M.F. Howland, Nat. Commun. 15 (1) (2024) 6658.
[119] H. Mian, F. Machot, H. Ullah, A. Keprate, M. Siddiqui, Renew. Sustain. Energy Rev. 224 (2025) 116098.
[120] D. Sarker, M. Sakif, T. Ngo, T. Das, IFAC-PapersOnLine 59 (30) (2025) 227–232.
[121] S. Guth, E. Katsidoniotaki, T.P. Sapsis, Wind Energy 27 (1) (2024) 75–100.
[122] S. Tang, B. Sweetman, J. Gao, Ocean Eng. 229 (2021) 108866.
[123] R.G. Budynas, J.K. Nisbett, et al., Shigley's Mechanical Engineering Design, vol. 9, McGraw-Hill New York, 2011.
[124] A. England, A. Toumpis, Y. Gorash, Metals 13 (11) (2023) 1860.
[125] F.C. Campbell, Fatigue and Fracture: Understanding the Basics, ASM International, 2012.
[126] B. Kühn, M. Lukic, A. Nussbaumer, H.-P. Günther, R. Helmerich, S. Herion, M.H. Kolstein, S. Walbridge, B. Androic, O. Dijkstra, et al., Assessment of Existing Steel Structures: Recommendations for Estimation of Remaining Fatigue Life, Joint Research Center, 2008.
[127] A. Palmgren, VDI. Z. 68 (1924) 339–341.
[128] M.A. Miner, Cumulative Damage in Fatigue, American Society of Mechanical Engineers, 1945.
[129] J. Slavič, M. Boltezar, M. Mrsnik, M. Cesnik, J. Javh, Vibration Fatigue by Spectral Methods: From Structural Dynamics to Fatigue Damage–Theory and Experiments, Elsevier, 2020.
[130] DNV-RP-C203: Fatigue Design of Offshore Steel Structures, Det Norske Veritas, 2011.
[131] P. Strzelecki, A. Mazurkiewicz, J. Musiał, T. Tomaszewski, M. Słomion, Materials 12 (22) (2019) 3677.
[132] O. Basquin, Proc. Amer. Soc. Test Mater., 10, 1910, pp. 625–630.
[133] C. Stromeyer, Proc. R. Soc. Lond. Ser. A Math. Phys. Char. 90 (620) (1914) 411–425.
[134] A. Palmgren, Z. Ver. Dtsch. Ing. (VDI Z.) (1924) 0341–7258.
[135] W. Weibull, W. Weibull, S. Physicist, W. Weibull, S. Physicien, W. Weibull, A Statistical Representation of Fatigue Failures in Solids, Elander, 1949.
[136] Y. Murakami, T. Takagi, K. Wada, H. Matsunaga, Int. J. Fatigue 146 (2021) 106138.
[137] F. Della Santa, G. Zorzi, A. Mehmanparast, Wind 4 (3) (2024) 251–274.
[138] Q. Wang, M.K. Khan, C. Bathias, Theor. Appl. Mech. Lett. 2 (3) (2012) 031002.
[139] J. Chen, S. Liu, W. Zhang, Y. Liu, Int. J. Fatigue 134 (2020) 105511.
[140] C. Rubiella, C.A. Hessabi, A.S. Fallah, Int. J. Fatigue 117 (2018) 230–245.
[141] I. Burhan, H.S. Kim, J. Compos. Sci. 2 (3) (2018) 38.
[142] W. Weibull, Fatigue Fract. Met. 4 (1952) 182–196.
[143] G. Sendeckyj, Test Methods and Design Allowables for Fibrous Composites, ASTM International, 1981.
[144] H.S. Kim, J. Zhang, J. Reinf. Plast. Compos. 20 (10) (2001) 834–848.
[145] M. Kawai, N. Itoh, J. Compos. Mater. 48 (5) (2014) 571–592.
[146] G. Miao, T. Sun, X. Wang, J. Phys.: Conf. Ser. 1605 (1) (2020) 012145.
[147] Standard, ASTM, E1049-85 (Reapproved 2017) Standard Practices for Cycle Counting in Fatigue Analysis, Tech. Rep., ASTM International, West Conshohocken, PA, 2017.
[148] T. Dirlik, Application of Computers in Fatigue Analysis (Ph.D. thesis), University of Warwick, 1985.
[149] D. Benasciutti, R. Tovo, Int. J. Fatigue 27 (8) (2005) 867–877.
[150] P. Wirsching, Int. J. Fatigue 2 (2) (1980) 77–83.
[151] G. Mesmacque, S. Garcia, A. Amrouche, C. Rubio-Gonzalez, Int. J. Fatigue 27 (4) (2005) 461–467.
[152] K. Hectors, W. De Waele, Metals 11 (2) (2021) 204.
[153] G. Zhao, Y. Liu, N. Ye, Int. J. Fatigue 156 (2022) 106636.
[154] Q. Xiao, X. Wang, D. Chen, X. Zhou, X. Liu, W. Yang, Int. J. Fatigue 191 (2025) 108709.
[155] C.S. Bandara, S.C. Siriwardane, U.I. Dissanayake, R. Dissanayake, Comput. Mater. Sci. 96 (2015) 96–101.
[156] D.S. Saini, D. Karmakar, S. Ray-Chaudhuri, J. Ocean Eng. Sci. 1 (3) (2016) 186–202.
[157] American Petroleum Institute, Planning, Designing, and Constructing Fixed Offshore Platforms: Working Stress Design, American Petroleum Institute, 2020.
[158] Dnv, G.L., DNVGL-ST-0126: Support Structures for Wind Turbines, DNV GL, Oslo, Norway, 2016.
[159] A. Kolios, L. Wang, A. Mehmanparast, F. Brennan, Ocean Eng. 178 (2019) 38–47.
[160] A.D. Oyegbile, M. Muskulus, Mar. Struct. 96 (2024) 103634.
[161] M. Efthymiou, Development of SCF Formulae and Generalised Influence Functions for Use in Fatigue Analysis, OTJ, 1988.
[162] M. Althaf, K.M. Navvar, G. Prakash, N. Varghese, C. Navaneeth, IOP Conf. Ser.: Mat. Sci. Eng. 1114 (1) (2021) 012009.
[163] P. Amirafshari, F. Brennan, A. Kolios, Wind Energy Sci. 6 (3) (2021) 677–699.
[164] A.A. Shittu, A. Mehmanparast, P. Hart, A. Kolios, Reliab. Eng. Syst. Saf. 215 (2021) 107838.
[165] C.G. Soares, Y. Garbatov, Mar. Struct. 9 (3–4) (1996) 495–516.
[166] E. Ayala-Uraga, T. Moan, Int. J. Fatigue 29 (3) (2007) 444–456.
[167] I. Lotsberg, G. Sigurdsson, A. Fjeldstad, T. Moan, Mar. Struct. 46 (2016) 167–192.
[168] V. Giannella, Int. J. Fract. 235 (2) (2022) 179–195.
[169] M. Mlikota, S. Staib, S. Schmauder, v. Božić, J. Phys.: Conf. Ser. 843 (1) (2017) 012042.
[170] N. Fantuzzi, R. Dimitri, F. Tornabene, Compos. Struct. 145 (2016) 162–185.
[171] S.-H. Ju, S. Liu, Compos. Struct. 81 (4) (2007) 614–621.
[172] K. Hectors, W. De Waele, J. Constr. Steel Res. 176 (2021) 106376.
[173] K. Walker, Effects of Environment and Complex Load History on Fatigue Life, ASTM International, 100 Barr Harbor Drive, PO Box C700, West Conshohocken, PA, 1970, pp. 1–14.
[174] S.M. Beden, S. Abdullah, A.K. Ariffin, Eur. J. Sci. Res. 28 (3) (2009) 364–397.
[175] Y. Yan, S.-H. Park, Int. J. Solids Struct. 45 (17) (2008) 4756–4765.
[176] D. Motamedi, S. Mohammadi, Int. J. Fract. 161 (2010) 21–39.
[177] S. Guo, X. Tian, Y. Tang, Mater. Today Commun. 40 (2024) 110158.
[178] R. Singh, A. Gupta, Int. J. Fatigue 10 (1) (1988) 49–53.
[179] J. Wu, SN Curves and Fracture Mechanics Based Fatigue Assessment of Offshore Floating Wind Turbines (Ph.D. thesis), Newcastle University, 2020.
[180] K. Doshi, T. Roy, Y.S. Parihar, Mar. Struct. 54 (2017) 1–22.
[181] P. Amirafshari, A. Kolios, Int. J. Fatigue 159 (2022) 106763.
[182] J. Stutzmann, L. Ziegler, M. Muskulus, Energy Procedia 137 (2017) 143–151.
[183] H. Wang, B. Li, J. Gong, F.-Z. Xuan, Eng. Fract. Mech. 284 (2023) 109242.
[184] D.P. Liu, G. Ferri, T. Heo, E. Marino, L. Manuel, Renew. Energy 225 (2024) 120238.
[185] K. Arvanitis, P. Nikolakopoulos, D. Pavlou, M. Farmanbar, Alex. Eng. J. 125 (2025) 55–66.
[186] X. Fang, G. Liu, H. Wang, Y. Xie, X. Tian, D. Leng, W. Mu, P. Ma, G. Li, Ocean Eng. 266 (2022) 112996.
[187] E. Branlard, J. Jonkman, C. Brown, J. Zhang, Wind Energy Sci. 9 (1) (2024) 1–24.
[188] J. Jorgensen, M. Hodkiewicz, E. Cripps, G.M. Hassan, Comput. Ind. 145 (2023) 103806.
[189] R. Kazacoks, P. Jamieson, Energy Procedia 80 (2015) 13–20.
[190] J. Gao, B. Sweetman, S. Tang, Ocean Eng. 261 (2022) 111921.
[191] F. Zhu, B. Yeter, F. Brennan, M. Collu, Eng. Struct. 318 (2024) 118759.
[192] E. Balli, Y. Zheng, Ocean Eng. 261 (2022) 112119.
[193] C. Ren, Y. Xing, Renew. Energy 215 (2023) 118977.
[194] J. Pacheco, F. Pimenta, S. Pereira, Á. Cunha, F. Magalhães, Eng. Struct. 285 (2023) 115913.
[195] T. Tao, Y. Yang, T. Yang, S. Liu, X. Guo, H. Wang, Z. Liu, W. Chen, C. Liang, K. Long, et al., Ocean Eng. 303 (2024) 117706.
[196] A. Fajuyigbe, Fracture mechanics analysis of offshore wind turbine monopile structures for lifetime extension, 2022.
[197] Y. Xi, H. Li, L. Sun, Z. Wang, Ocean Eng. 300 (2024) 117180.
[198] T. Chen, W. Li, R. Deng, H. Zuo, Ocean Eng. 314 (2024) 119786.
[199] M. Peng, M. Liu, Y. Cong, S. Gu, Ocean Eng. 302 (2024) 117751.
[200] N. Dimitrov, A. Natarajan, M. Kelly, Wind Energy 18 (11) (2015) 1917–1931.
[201] B. Kosović, S. Basu, J. Berg, L.K. Berg, S.E. Haupt, X.G. Larsén, J. Peinke, R.J. Stevens, P. Veers, S. Watson, Wind Energy Sci. Discuss. 2025 (2025) 1–67.
[202] A. Nybø, F.G. Nielsen, J. Reuder, M.J. Churchfield, M. Godvik, Wind Energy 23 (9) (2020) 1810–1830.
[203] G. Dodet, S. Abdalla, M. Alday, M. Accensi, J. Bidlot, F. Ardhuin, J. Atmos. Ocean. Technol. 39 (7) (2022) 887–901.
[204] S. Yang, X. Deng, M. Zhang, Y. Xu, Ocean Eng. 267 (2023) 113222.
[205] S. Perez-Becker, F. Papi, J. Saverin, D. Marten, A. Bianchini, C.O. Paschereit, Wind Energy Sci. 5 (2) (2020) 721–743.
[206] M.B. Van Der Meulen, T. Ashuri, G.J. Van Bussel, D.P. Molenaar, The Science of Making Torque from Wind, Oldenburg, Germany, 2012, pp. 1–10.
[207] K. Xu, Y. Shao, Z. Gao, T. Moan, J. Fluids Struct. 88 (2019) 216–240.
[208] A. Mackojc, K. Mackojc, R. McGowan, N. Barltrop, Energies 19 (1) (2025) 169.
[209] B. Ruan, C. Liu, S. Wang, R. Xi, Thin-Walled Struct. (2026) 114487.